Università di Foggia

Department of Medical Science and Surgery

PhD COURSE IN INNOVATIVE SCIENCE AND TECHNOLOGIES FOR HEALTH

XXXVII Cycle

Dis-connectome Biomarkers after Acute Stroke

Predicting 12-Month Functional Independence, Motor Recovery, and Spasticity

Doctoral Coordinator:

Prof.ssa Elena Ranieri

Tutor:

Prof. Santamato Andrea

PhD Student

Dott.ssa Stefania Spina

Anno Accademico 2024/2025

Sei Amore, Luce, Vita.

Ammiro Te Oltre ogni Ragione ed Emozione.

ABSTRACT

Background: Stroke is a leading cause of long-term adult disability, yet recovery is highly heterogeneous and difficult to predict on an individual basis. Conventional prognostic markers, such as initial clinical severity and lesion volume, have limited accuracy, failing to capture the complex network-level consequences of a focal brain injury. The connectome framework, which models stroke as a disruption of large-scale brain networks, offers a more mechanistic approach to understanding post-stroke deficits. However, the prognostic value of a comprehensive set of structural disconnectome metrics for specific, long-term clinical outcomes remains largely unvalidated, representing a critical gap in translating advanced neuroimaging into clinical practice.

Aim: The primary aim of this thesis was to investigate whether a comprehensive set of structural disconnectome and lesion geometry metrics, derived from routinely acquired acute-phase clinical scans, could accurately and independently predict functional independence, ambulatory status, and the development of spasticity at 12 months post-stroke.

Materials and Methods: In a longitudinal cohort of 28 stroke survivors (ischemic and hemorrhagic), acute-phase CT or MRI scans were used to segment lesions. These patient-specific lesion masks were virtually overlaid onto a normative healthy connectome atlas to compute structural disconnectome maps. A comprehensive set of predictive features was derived, including: (1) lesion geometry metrics (Lesion Volume, Lesion Surface, Bounding Box Volume, Ratio of Bounding Box to Lesion Volume, and Lesion Sphericity); (2) global and network-level disconnection metrics (loss in Global Efficiency, disconnection within the Somatomotor network, Inter-Hemispheric motor disconnection, and disconnection from motor to frontoparietal/dorsal attention networks); (3) nodal disconnection metrics for key sensorimotor regions (M1, S1, SMA, PMd, Thalamus); and (4) composite and laterality indices (Motor Network Disconnection Index, M1 and SMA Laterality Indices). Multivariate predictive models were developed for 12-month outcomes (modified Rankin Scale

[mRS], Functional Ambulation Classification [FAC], Modified Ashworth Scale [MAS]) and for continuous motor recovery (change in NIHSS motor score). Model performance was assessed and validated using cross-validation techniques.

Results: Predictive models combining baseline clinical severity (NIHSS motor score) with imaging metrics consistently outperformed imaging-only specifications. Distinct predictive signatures emerged for each outcome. Functional independence (mRS ≤ 2) was best predicted by a model including Lesion Sphericity and MNDI3 (AUC = 0.974). Ambulatory independence (FAC ≥ 4) was dominated by the SMA Laterality Index and Global Efficiency loss (AUC = 0.952). In contrast, the presence of spasticity was most strongly predicted by the initial NIHSS motor score, with a secondary contribution from disconnection within the motor network (AUC = 0.771). Continuous motor recovery was substantially explained by a combined model including lesion volume and MNDI3 ($R^2 = 0.66$), whereas an imaging-only model performed poorly ($R^2 \approx 0.22$).

Discussion: The findings suggest that while the initial severity of corticospinal injury is the primary driver of maladaptive plasticity leading to spasticity, the ultimate ceiling of functional and ambulatory recovery is more closely tied to the topological characteristics of the brain injury. The predictive power of lesion geometry and network asymmetry underscores the importance of widespread, multi-system disruption for global disability and the critical role of interhemispheric balance for complex motor tasks like gait. The independent prognostic value of disconnectome metrics demonstrates their ability to capture mechanistic aspects of neural injury not fully represented by clinical scores alone.

Conclusion: Structural disconnectome metrics are powerful, independent, and outcome-specific biomarkers for long-term recovery after stroke. This work provides a robust framework for integrating network neuroscience into clinical prognostication, representing a critical step towards the development of personalized and stratified neurorehabilitation strategies.

TABLE OF CONTENTS

CHAPTER 1: INTRODUCTION

1.1 The Clinical Challenge: Heterogeneity and Unpredictability in Post-Stroke Recovery

Stroke represents a paramount global health challenge, defined not merely by its acute mortality but by its enduring legacy as the leading cause of long-term adult disability worldwide[1]. Annually, millions of individuals survive the initial cerebrovascular event only to face a lifetime of neurological sequelae that profoundly alter the trajectory of their lives, imposing a staggering socio-economic burden on patients, caregivers, and healthcare systems. The clinical aftermath of stroke is a complex syndrome encompassing a wide spectrum of potential deficits, including motor impairments such as hemiparesis, sensory loss, cognitive dysfunction, aphasia, and the development of secondary complications like spasticity and chronic pain[2]. This clinical reality presents a formidable prognostic challenge: the recovery trajectory following stroke is profoundly heterogeneous. Even when controlling for initial injury severity and key patient demographics, the variance in long-term functional outcomes remains vast. Two patients with seemingly comparable initial clinical presentations and lesion characteristics can embark on dramatically different recovery paths, with one achieving near-complete functional independence while the other remains severely disabled. This vast, unexplained variance makes accurate, individual-level prediction a persistent and critical unmet need in clinical neurology.

For decades, the cornerstones of stroke prognostication have been a limited set of conventional markers, primarily patient age, the initial severity of the neurological deficit as quantified by the National Institutes of Health Stroke Scale[3,4] or Fugl-Meyer scale[5], and the volume of the infarct as measured on neuroimaging[6,7]. While these variables are statistically powerful predictors at a population level and remain indispensable in acute clinical decision-making, they often function as blunt instruments when applied to the individual patient[8]. They provide a coarse estimate of outcome but lack the precision required to guide personalized rehabilitation strategies or to offer patients and their families a reliable prognosis. The limitations of this traditional, lesion-centric model are particularly evident in the well-documented, yet poorly understood, disconnect between lesion

volume and functional outcome[9]. This prognostic uncertainty does not simply represent a gap in our predictive capabilities; it reflects a fundamental limitation in the conceptual framework itself, necessitating a paradigm shift from viewing stroke as a focal anatomical injury to understanding it as a systemic disruption of the brain's complex network architecture.

The resolution to this clinical and scientific paradox lies in a paradigm shift, moving away from a purely topographical view of brain damage towards a network-based understanding of its consequences. This modern framework conceptualizes the brain not as a mosaic of independent functional modules, but as a single, massively interconnected network—the human connectome. The word connectome was coined by Olaf Sporns[10] and refers to the complete set of structural connections between neurons of the brain. The connectome provides the complete architectural blueprint of the brain, encompassing both the structural connectivity (the anatomical white matter pathways that form the brain's physical wiring) and the functional connectivity (the dynamic patterns of synchronized communication between distributed brain regions).

Consequently, a focal stroke inflicts damage that radiates far beyond its anatomical borders. The lesion acts as an epicenter of network disruption, causing not only the direct transection of pathways passing through it but also inducing remote dysfunction in structurally intact but connected brain regions—a phenomenon historically termed diaschisis. The complete map of these network-level disruptions is known as the disconnectome. This construct provides a powerful, mechanistic link between the focal anatomical injury and the widespread, often syndromic, clinical deficits observed in patients. It posits that the specific pattern of network disconnection, rather than lesion volume alone, is the more fundamental determinant of a patient's clinical presentation and, crucially, their ultimate capacity for recovery[11]. This network-based perspective not only reframes our understanding of stroke pathophysiology but, most critically, provides a new and powerful lens through which to approach the challenges of rehabilitation and prognostication.

1.2 The Rehabilitative Imperative: Why Network-Level Prognosis is Crucial

The ultimate goal of stroke care extends beyond acute survival to the maximization of long-term functional recovery, a domain primarily addressed through rehabilitation[12]. Modern neurorehabilitation is conceptualized not as a generic set of exercises, but as a targeted intervention designed to harness and guide the brain's intrinsic capacity for neuroplasticity. However, for this process to be maximally effective, it must be guided by an accurate and early understanding of an individual's potential for recovery. This transforms prognostication from a passive act of predicting the future into an active, indispensable tool for informing present-day therapeutic strategy[13,14].

A robust, network-level prognosis holds the potential to revolutionize rehabilitation by enabling a shift from a one-size-fits-all approach to a truly personalized and stratified model of care. For instance, by quantifying the structural integrity of the corticospinal tract and other key motor pathways, clinicians could better define realistic therapeutic goals. A patient with a severely disconnected motor system might benefit from an early focus on compensatory strategies and assistive technologies, thereby avoiding the frustration and resource expenditure of intensive restorative therapies with a low probability of success. Conversely, a patient with a preserved, albeit functionally silent, motor network could be triaged for aggressive, high-dose restorative interventions designed to re-engage dormant circuits.

Furthermore, accurate prediction allows for the stratification of patients for preventative therapies. The development of spasticity, a debilitating and common complication driven by maladaptive plasticity, is a prime example. Identifying individuals at the highest risk of developing severe spasticity based on their specific pattern of network disconnection could justify early and aggressive interventions—such as targeted pharmacological treatments, focal botulinum toxin injections, or specific physical therapy regimens—aimed at mitigating its onset and severity before it becomes entrenched.

Ultimately, this approach enables the personalization of therapy at a mechanistic level. Understanding which specific networks are disrupted—whether the primary damage lies within the core sensorimotor network, in the pathways connecting motor and cognitive control systems, or in the interhemispheric balance—could guide the very nature of the rehabilitation provided. This could inform the choice between intensive motor practice, cognitive rehabilitation, non-invasive brain stimulation targeting specific nodes, or a combination[15]. Despite this immense clinical potential, a critical gap exists: the current rehabilitative landscape lacks robust, validated, and, most importantly, clinically feasible biomarkers derived from the connectome to guide these crucial, patient-specific decisions.

1.3 Rationale, Aims, and Structure of this Thesis

Given the established limitations of conventional prognostic markers and the clear imperative to ground rehabilitative strategies in the underlying neurobiology of recovery, this thesis is predicated on the need to validate the clinical utility of connectome-based biomarkers. My clinical background as a physiatrist has provided me with a firsthand perspective on the profound heterogeneity of stroke recovery and the daily challenges of formulating effective, individualized rehabilitation plans in the face of prognostic uncertainty. This clinical experience has been the driving force behind the research conducted over the past three years of my doctoral studies. The central rationale is that by bridging the gap between advanced neuroimaging and clinical rehabilitation, we can move towards a more mechanistic and precise approach to patient care. This work leverages the structural disconnectome as a potential tool to achieve this, testing its capacity to provide a more granular and biologically plausible prognosis than is currently possible.

The primary aim of this dissertation is therefore to investigate whether structural disconnectome metrics, derived from standard, acutely acquired clinical brain scans, can accurately and independently predict key 12-month outcomes after stroke. This overarching goal is broken down into three specific objectives:

- To quantify the structural disconnectome in a cohort of patients with stroke and characterize its impact on diverse neural networks.
- To develop and validate multivariate predictive models for long-term functional independence.
- To develop and validate models for long-term ambulatory independence.
- To develop and validate models for the subsequent development of spasticity.

The central hypothesis is that disconnectome metrics will provide significant and independent prognostic value, superior to that of conventional clinical and volumetric (lesion volume) predictors, across all three clinical endpoints.

To address these aims, this thesis is structured as follows. **Chapter 2** will provide a detailed overview of the theoretical background, defining stroke, the principles of neuroplasticity, and the methodologies for mapping the human connectome. **Chapter 3** will describe the methods employed in this study, including the patient cohort, the clinical and imaging protocols, the pipeline for lesion segmentation and disconnectome generation, and the statistical framework for predictive modeling. **Chapter 4** will present the primary results, detailing the descriptive characteristics of the cohort and the performance of the predictive models for each clinical outcome. Finally, **Chapter 5** will discuss the interpretation and clinical implications of these findings, address the study's limitations, and propose future directions for research in this emerging field.

CHAPTER 2 - STROKE AND THE CONNETOME

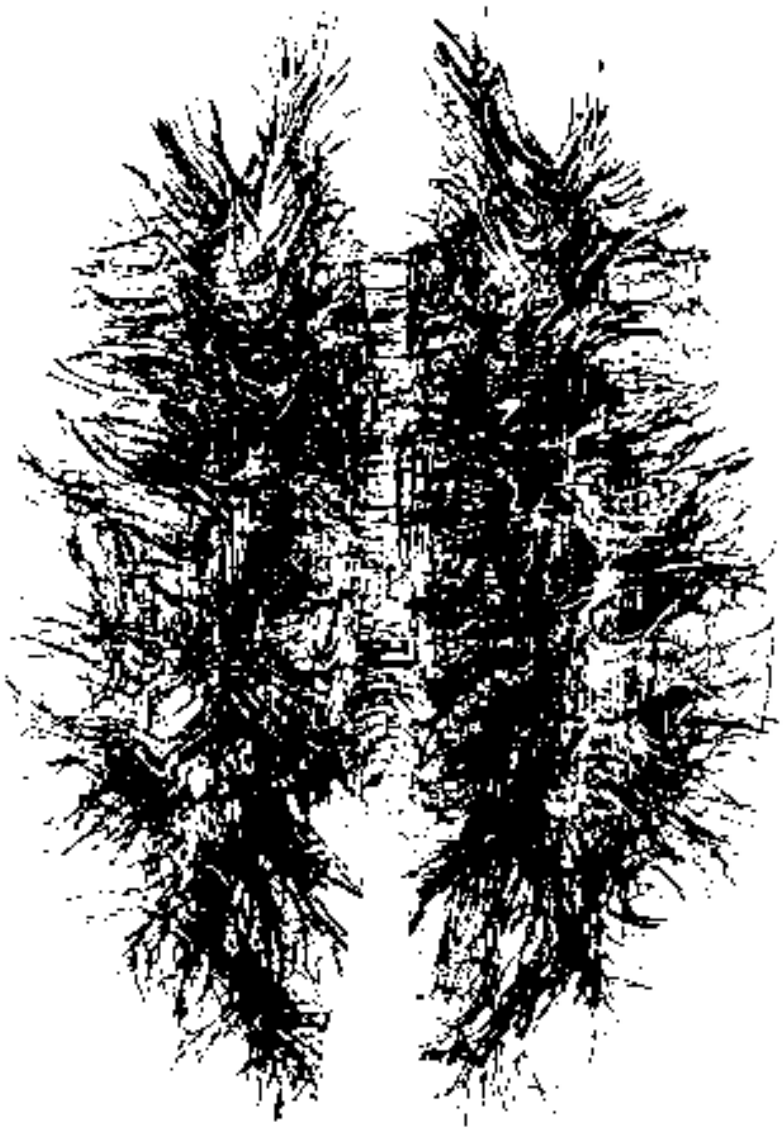

Stroke represents a paramount global health challenge, constituting the second-leading global cause of mortality and a primary cause of complex long-term disability. According to the most recent Global Burden of Disease (GBD) 2019 data, over 12.2 million new strokes occur annually, contributing to a prevalent population of over 101 million stroke survivors[16]. This translates into a staggering 143 million disability-adjusted life years (DALYs) lost globally each year, with a disproportionate impact on low- and middle-income countries[17]. The associated socio-economic burden is immense, with global costs related to direct healthcare, rehabilitation, and lost productivity estimated to exceed US$721 billion annually[18].

While the etiology is multifactorial, high systolic blood pressure remains the single most important modifiable risk factor, accounting for approximately 55.5% of all stroke-related DALYs. Other major contributors include high BMI (24.3%), high fasting plasma glucose (20.2%), ambient particulate pollution (20.1%), and smoking (17.6%)[19]. Crucially, as the global population ages, the absolute number of stroke survivors living with significant neurological sequelae is projected to increase. This is underscored by the current global lifetime risk of stroke, which now stands at one in four for individuals over the age of 25[20], highlighting the urgent need for more accurate prognostic models to guide clinical management and resource allocation.

2.1 Stroke: definition and classification

The contemporary understanding of stroke is anchored in a precise, tissue-based definition that has evolved significantly from its historical, purely clinical origins[21]. Stroke is now formally defined as an acute episode of neurological dysfunction attributable to a focal vascular cause, resulting in infarction of central nervous system tissue. This seminal redefinition by the American Heart Association/American Stroke Association (AHA/ASA) marked a paradigm shift away from the traditional World Health Organization (WHO) criterion, which relied on symptom duration (lasting >24 hours) as the primary differentiator[22]. The advent of high-resolution neuroimaging, particularly

diffusion-weighted magnetic resonance imaging (DWI), rendered this arbitrary temporal threshold obsolete by demonstrating that many transient neurological episodes resulted in objective evidence of cellular death. Thus, the central criterion shifted from symptom duration to the presence of tissue injury. This tissue-based definition concurrently refined the concept of a Transient Ischemic Attack (TIA) as a transient episode of neurological dysfunction without evidence of acute infarction. This modern, pathologically grounded definition provides the essential foundation upon which the clinical classification and pathophysiological mechanisms of stroke are built.

This clinical classification is fundamentally predicated on the distinction between ischemic and haemorrhagic etiologies. Ischemic stroke, which constitutes the vast majority of cases, is etiologically subtyped according to the widely adopted TOAST (Trial of Org 10172 in Acute Stroke Treatment) classification[23,24]. This system delineates five primary categories: large-artery atherosclerosis, cardioembolism, small-vessel occlusion (lacunar stroke), stroke of other determined etiology, and stroke of undetermined etiology. A significant evolution in this framework has been the recognition of Embolic Stroke of Undetermined Source (ESUS), a construct that refines the latter category by identifying patients whose strokes are likely embolic but lack a definitive cardioembolic or arterial source, thereby guiding secondary prevention strategies. In contrast, hemorrhagic stroke is categorized first by location—primarily as intracerebral hemorrhage (ICH) or subarachnoid hemorrhage (SAH)—and second by cause[25]. ICH is further stratified into primary hemorrhages, typically arising from hypertensive vasculopathy in deep brain structures or cerebral amyloid angiopathy in lobar regions, and secondary hemorrhages due to underlying pathologies such as vascular malformations or tumors[26].

2.2 Stroke: Recovery and the Neuroplasticity

The clinical trajectory following stroke is profoundly heterogeneous, yet it is underpinned by fundamental biological principles of neuroplasticity[27]. Spontaneous recovery is most dynamic within the first three to six months post-ictus, a critical window during which the majority of functional gains

are observed, followed by a more gradual plateau phase[28]. The primary clinical challenge is the accurate prognostication of this recovery course for an individual patient. Traditionally, prognostication has relied on a limited set of variables, primarily initial stroke severity (as measured by the NIHSS), patient age, and lesion volume[29]. However, these traditional markers, while statistically significant at a population level, often possess insufficient predictive power for individual outcomes. A growing body of evidence indicates that lesion volume is a less potent predictor than lesion topography, as small, strategically located lesions can cause disproportionately severe deficits by disrupting critical neural pathways. This highlights a fundamental limitation: conventional prognostic tools are crude proxies for the complex, network-level disruption that truly dictates a patient's capacity for recovery[30,31].

The neurobiological substrate for this recovery is neuroplasticity, the brain's intrinsic capacity for structural and functional reorganization in response to injury[32]. In the immediate aftermath of stroke, recovery is partly driven by the resolution of acute pathological processes, including the reperfusion of the ischemic penumbra and the resolution of diaschisis—the remote functional depression of structurally intact brain regions connected to the infarct. Long-term recovery, however, depends on a more profound and enduring reorganization of neural circuitry. At a microstructural level, these mechanisms include axonal sprouting, where surviving neurons form new connections; synaptogenesis, the creation of new synapses; and alterations in dendritic arborization. At a macrostructural, systems level, functional recovery is associated with the topological reorganization of large-scale brain networks. This involves the remapping of cortical representations of function, the recruitment of secondary or vicarious neural pathways (often in perilesional or homologous contralateral regions), and a dynamic shift in interhemispheric balance. The interplay between inhibitory and excitatory influences between the two hemispheres is a critical modulator of motor recovery, with ongoing debate surrounding the roles of interhemispheric competition versus vicarious functional takeover.

Consequently, post-stroke recovery is not merely a process of local tissue repair but a complex, network-wide phenomenon. The brain's ability to reorganize is constrained by the surviving anatomical architecture. The initial lesion and, more importantly, the resulting structural disconnectome, define the residual substrate upon which all subsequent neuroplastic processes must operate. Therefore, a direct quantification of this network damage offers a more mechanistic and biologically plausible approach to prognostication than simple volumetric or clinical assessments. We posit that the structural disconnectome serves as a powerful, patient-specific biomarker, capable of predicting the long-term potential for functional independence, the ceiling of motor recovery, and the likelihood of developing maladaptive plasticity, such as spasticity, by providing a direct measure of the structural integrity of the networks essential for recovery.

2.3 A Paradigm Shift: Stroke as a Disease of the Brain Connectome

The traditional, lesion-centric view of stroke—which has historically correlated clinical deficits primarily with the volume and location of infarcted tissue—is undergoing a profound paradigm shift. This evolution is driven by a more sophisticated understanding of the brain not as a collection of quasi-independent functional modules, but as a massively interconnected network: the connectome. The connectome provides a multi-scalar architectural framework, spanning the microscopic level of individual synapses, the mesoscopic level of local circuit and inter-regional projections, and the macroscopic level of large-scale white matter tracts that can be mapped in vivo using advanced neuroimaging techniques like diffusion tensor imaging (DTI)[10]. From this perspective, a stroke is no longer viewed merely as a focal parenchymal injury, but as an acute, catastrophic disruption of the brain's intricate wiring diagram.

As cogently articulated by Silasi and Murphy, the impact of a cerebrovascular event on the connectome is both immediate and far-reaching[11]. The initial ischemic cascade leads to direct neuronal loss within the infarct core, causing the physical transection of axonal pathways. This constitutes direct disconnection, the severing of the anatomical "highways" that pass through the

lesion. However, the true explanatory power of the connectome paradigm lies in its ability to account for remote network dysfunction. The phenomenon of diaschisis[33]—the functional depression of structurally intact brain regions anatomically connected to the infarct—is powerfully reframed as a predictable consequence of network disruption. This indirect disconnection arises from the loss of excitatory afferent input and the subsequent functional uncoupling of nodes that are critical for network operations, even if they are located far from the primary lesion site.

The quantifiable map of these network-level disruptions is termed the disconnectome. This construct allows for a patient-specific, mechanistic understanding of stroke pathophysiology. The structural disconnectome specifically maps the probability of white matter pathways being damaged by the lesion, typically derived by embedding a patient's specific lesion mask onto a normative atlas of the human structural connectome. This anatomical damage, in turn, precipitates widespread alterations in the functional connectome, which is characterized by the statistical interdependence (e.g., temporal correlation) of activity between distributed brain regions. Post-stroke, this manifests as a canonical pattern of functional network pathology, including a profound weakening of interhemispheric functional connectivity, an intensification of intra-hemispheric segregation, and a global reduction in network modularity.

This framework provides a compelling explanation for the observed low-dimensional structure of post-stroke behavioral deficits. The clinical observation that disparate functional impairments (e.g., in motor, language, and attentional domains) frequently co-occur and covary is no longer viewed as coincidental but as a direct reflection of the disruption of large-scale, multifunctional networks upon which these abilities collectively depend. Therefore, the disconnectome serves as a mechanistic bridge, linking a focal anatomical injury to a global, syndromic clinical presentation. It posits that the topography of network disruption, rather than simple lesion volume, is the more critical determinant of clinical outcome. The surviving anatomical architecture, as defined by the structural disconnectome, represents the essential substrate upon which all subsequent processes of

neuroplasticity and recovery must operate. Consequently, its quantification offers a powerful and biologically plausible foundation for prognostic modeling, moving beyond correlational clinical variables to a direct, patient-specific measure of network integrity.

2.4 Methodologies for Mapping the Human Connectome in vivo

The conceptual leap from the brain as a set of regions to a fully integrated network has been propelled by transformative advances in non-invasive neuroimaging. Mapping the macroscopic human connectome has become a feasible scientific endeavor, primarily relying on two complementary magnetic resonance imaging modalities: one designed to elucidate the brain's structural architecture and another to capture its intrinsic functional dynamics[34].

The principal technique for mapping the structural connectome in vivo is Diffusion-Weighted Magnetic Resonance Imaging (dMRI)[35]. This method is uniquely sensitive to the microscopic, thermally-driven motion of water molecules. While this diffusion is isotropic within unconstrained spaces like the cerebrospinal fluid, the microstructural environment of white matter imposes significant directional constraints[36]. The axonal membranes and myelin sheaths that constitute fiber bundles create formidable barriers, compelling water to diffuse preferentially along their longitudinal axis. This directionally-dependent motion is termed anisotropy, and its quantification provides a powerful indirect probe of white matter organization and integrity[37].

The most established analytical framework for dMRI data is Diffusion Tensor Imaging (DTI), which models the diffusion profile within each voxel as a three-dimensional ellipsoid or tensor[38]. This tensor is fully described by its principal axes (eigenvectors) and their corresponding magnitudes (eigenvalues), from which several critical metrics are derived. Fractional Anisotropy (FA) is a widely used scalar index, ranging from 0 to 1, that quantifies the degree of directional coherence of diffusion and serves as a robust proxy for white matter integrity. This is complemented by measures such as Mean Diffusivity (MD), which reflects the overall magnitude of water mobility and is sensitive to

changes in tissue cellularity and edema, as well as Axial and Radial Diffusivity (AD and RD), which offer more specific inferences about axonal health and myelination, respectively[39]. Based on this voxel-wise directional information, computational algorithms known as tractography are employed to reconstruct the three-dimensional trajectories of white matter pathways. These algorithms operate by propagating streamlines from seed regions, following the principal diffusion orientations to chart the course of major fiber bundles. While deterministic approaches trace a single, most-likely path, more advanced probabilistic methods generate a distribution of potential pathways, thereby offering a more robust representation in brain regions with complex fiber architectures, such as areas of crossing or fanning fibers. The ultimate output is a comprehensive, brain-wide map of anatomical connections, often distilled into a structural connectivity matrix where nodes represent anatomically defined brain regions and edges are weighted by the density or number of connecting streamlines[40–43].

Complementing this structural map is the study of the brain's functional architecture, which is predominantly investigated using resting-state functional MRI (rs-fMRI)[44]. Functional connectivity is defined not by physical links, but by the statistical interdependence of neurophysiological signals over time. The rs-fMRI technique measures these dependencies via the Blood Oxygen Level-Dependent (BOLD) signal, an indirect proxy for neuronal activity[45,46]. It has been robustly demonstrated that spontaneous, low-frequency fluctuations in the BOLD signal are not random noise but are tightly correlated across anatomically separate regions. These correlations reveal the existence of a limited set of large-scale, intrinsically organized Resting-State Networks (RSNs), such as the Default Mode and Sensorimotor networks. Analytical approaches, ranging from seed-based correlation analyses to data-driven methods like Independent Component Analysis (ICA), are used to parse the complex whole-brain signal into these distinct functional systems. The resulting functional connectivity matrix, where edge weights represent the strength of temporal correlation between

nodes, provides a dynamic "snapshot" of the brain's intrinsic functional organization and its preferred patterns of inter-regional communication.

2.5 From Individual Mapping to Normative Connectomics

While the direct, individual-level mapping of structural and functional connectivity provides the most granular data, its application in the context of acute stroke research is fraught with profound practical and methodological challenges[47]. The acquisition of high-quality, high-angular resolution diffusion MRI suitable for advanced tractography is time-consuming and sensitive to patient motion, making it often unfeasible in the hyperacute clinical setting. More fundamentally, the ischemic lesion itself introduces a critical confound: the infarct core represents a void of destroyed tissue through which tractography algorithms cannot propagate, thus preventing the direct measurement of pathways that have been severed.

To circumvent these limitations, the field has increasingly adopted a powerful and elegant approach known as normative connectomics or lesion-network mapping[48]. This methodology, which is central to the work presented in this thesis, leverages the wealth of high-quality data from large-scale normative databases, such as the Human Connectome Project (HCP)[49,50] (https://www.humanconnectome.org). These projects provide detailed, high-resolution structural and functional connectome atlases, meticulously constructed from hundreds of healthy individuals, which serve as a "gold standard" reference for the intact human brain's architecture.

The core of this technique involves a process of virtual lesioning[51]. The methodology begins with the acquisition of standard, clinically available scans from the stroke patient, such as T1-weighted or FLAIR MRI sequences. From these images, the patient's specific lesion is carefully segmented to create a three-dimensional binary mask. This lesion mask is then spatially normalized into a standard stereotactic space (e.g., MNI space), a process that allows for its precise alignment with the normative connectome atlas. By digitally overlaying the patient-specific lesion mask onto this normative

structural atlas, one can identify the complete set of white matter streamlines that would have passed through the now-damaged tissue.

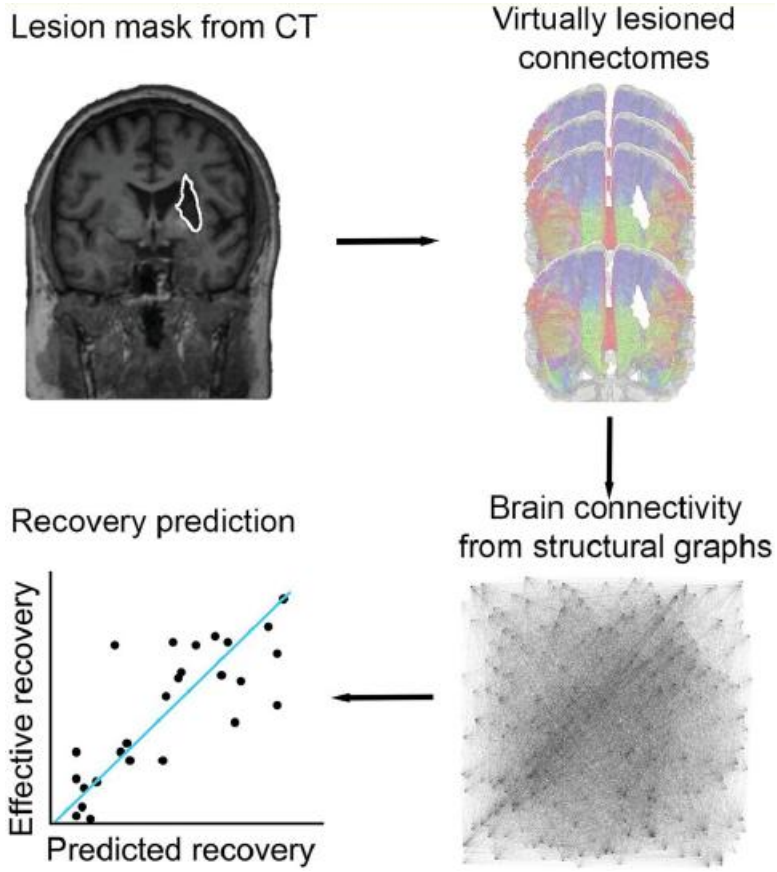

Figure 1 - Workflow for predicting recovery using virtually lesioned connectomes.

This set of intersected streamlines constitutes the patient's inferred structural disconnectome. This approach ingeniously bypasses the problem of mapping through the lesion by estimating the pre-morbid connectivity that was disrupted. The primary advantage of this technique is its clinical feasibility; it enables the quantification of complex, network-level damage using only the standard structural scans acquired during routine clinical care. It is this robust and innovative methodology that is employed throughout this thesis to quantify patient-specific network disruption and to test the hypothesis that the resultant disconnectome serves as a superior biomarker for long-term functional prognosis.

CHAPTER 3 - MATERIALS AND METHODS

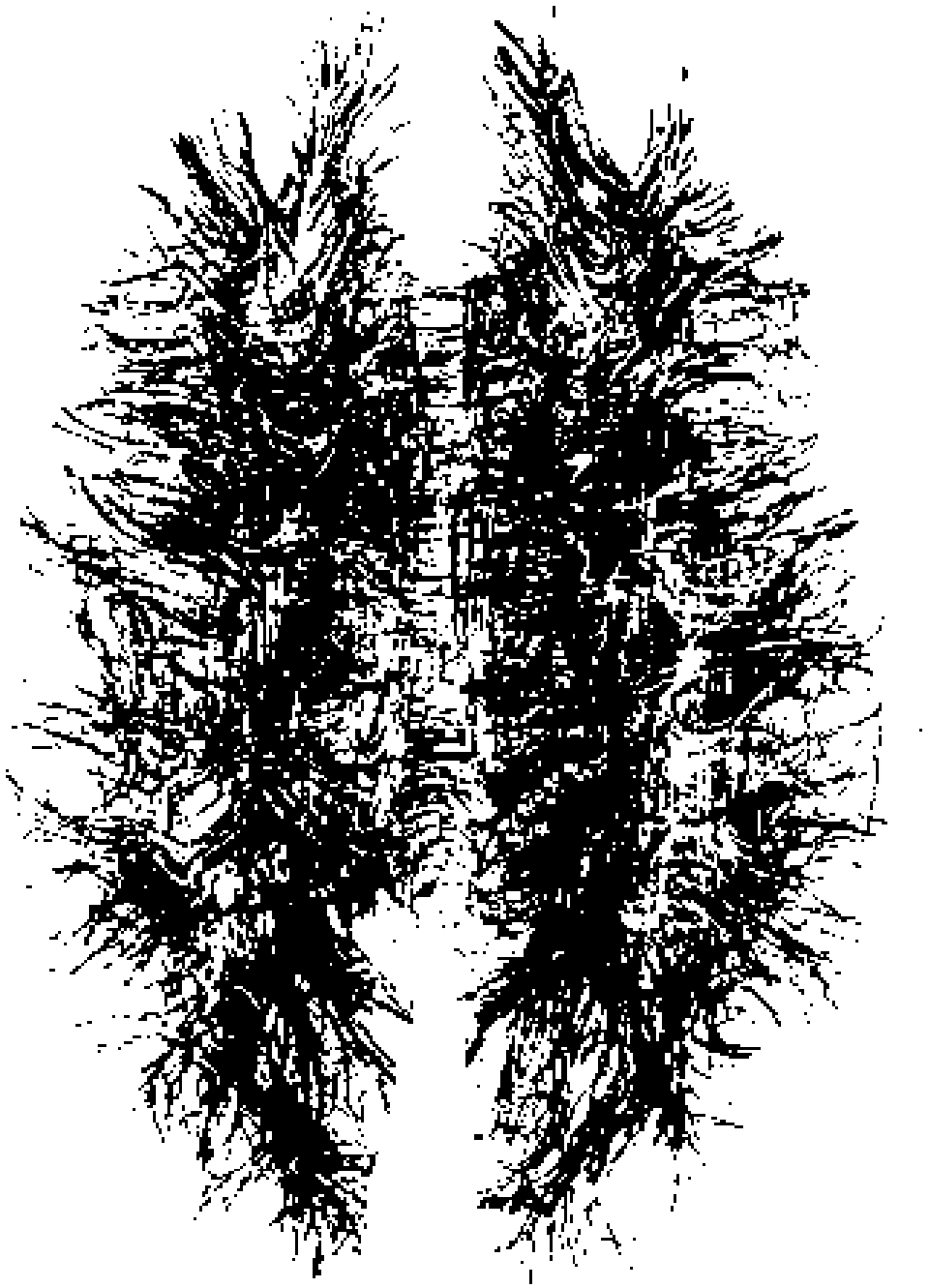

3.1 Study design and participants

This was a prospective, single-centre observational cohort conducted at Azienda Ospedaliero-Universitaria "Ospedali Riuniti" di Foggia (Italy). From June 1, 2023 to June 30, 2024, we screened all acute-stroke patients for whom the Neurology Stroke Unit requested a Physical and Rehabilitation Medicine consult. Eligible patients were approached by the PRM team for enrolment and scheduled for 12-month follow-up after the index event (±30 days). All patients received standard clinical care; no study intervention was performed. A subacute CT or MRI acquired 3–15 days after onset was used for lesion delineation and disconnectome analyses. Written informed consent was obtained from all participants or legal representatives.

Inclusion criteria

- Age ≥18 years.
- First-ever clinical stroke (index event), ischemic infarction or intracerebral hemorrhage.
- Unilateral hemispheric involvement (left or right) with a single focal lesion allowing clear lateralization.
- Availability of subacute CT or MRI at 7–15 days post-onset, suitable for lesion segmentation and MNI normalization.
- Feasibility of 12-month clinical follow-up (±30 days).
- For imaging analyses: acceptable-quality lesion mask after registration to MNI space.

Exclusion criteria

- History of prior stroke (clinical or imaging evidence) or multifocal acute lesions precluding a single index lesion.

- Primary subarachnoid hemorrhage, cerebral venous thrombosis, or global hypoxic–ischemic injury.
- Diffuse bilateral hemispheric injury or posterior fossa–dominant patterns where unilateral lateralization is not possible (investigator judgment).
- Pre-existing major neurological disease likely to confound outcomes (e.g., neurodegenerative disease, multiple sclerosis, prior severe TBI, brain tumour).
- Poor-quality imaging preventing reliable lesion segmentation/normalization (e.g., marked motion, extensive metal artefacts).
- Lack or withdrawal of informed consent.

3.2 Clinical assessments and outcomes

Clinical evaluations were coordinated by the Physical and Rehabilitation Medicine service in collaboration with the Neurology Stroke Unit. To align clinical phenotyping with subacute imaging and disconnectome analyses, we adopted a two-timepoint schedule. A baseline examination (T0) was performed during the subacute admission, within 24 hours of the 7–15-day imaging window. A follow-up visit at 12 months (T12 ±30 days) was conducted in the rehabilitation clinic. Examiners were not exposed to disconnectome metrics at the time of rating.

At T0 we recorded demographics and vascular history (age, sex, hypertension, diabetes, dyslipidaemia, atrial fibrillation, smoking), stroke characteristics (ischaemic vs intracerebral haemorrhage), lesion laterality (left/right), and imaging modality (CT vs MRI). The lesion volume (mL) was derived from the manually segmented mask after spatial normalisation to MNI and was retained as a clinically relevant covariate.

Neurological impairment was quantified with the National Institutes of Health Stroke Scale (NIHSS; 0–42, higher scores indicate greater impairment[4]) at T0 and T12. To isolate motor paresis, we derived

a motor subscore by summing item 5 (motor arm, affected side, 0–4) and item 6 (motor leg, affected side, 0–4), yielding NIHSS_motor on a 0–8 scale (0 = no motor deficit; 8 = complete arm-and-leg paresis). Motor recovery was defined a priori as the change from baseline:

$$\Delta \text{ NIHSS motor} = \text{NIHSS motor T12} - \text{NIHSS motor T0}$$

Global disability at 12 months was captured with the modified Rankin Scale (mRS; 0–6), an ordinal measure of functional dependence that summarises the level of assistance required in daily life. Briefly, 0 = no symptoms; 1 = no significant disability despite symptoms; 2 = slight disability (independent for personal affairs); 3 = moderate disability (some help required); 4 = moderately severe disability (unable to walk or attend to bodily needs without assistance); 5 = severe disability (bedbound, constant care); 6 = death[52,53]. In line with contemporary practice, we defined functional independence as mRS ≤2 at T12 and used this binary endpoint in primary analyses. When T12 could not be performed in person, mRS was collected by validated telephone interview; other scales were obtained in person.

Ambulatory status at 12 months was assessed with the Functional Ambulation Category (FAC; 0–5), an ordinal rating of the level of physical support or supervision required during walking. In brief, 0 = non-ambulatory; 1 = needs continuous physical assistance; 2 = needs intermittent/light assistance; 3 = requires supervision/verbal cueing only; 4 = independent on level surfaces (no physical contact or supervision); 5 = independent on all surfaces, including uneven terrain and stairs[54,55]. We prespecified FAC ≥4 as the cut-off for ambulatory independence, providing a clinically interpretable binary outcome complementary to mRS.

Spasticity was evaluated at T12 using the Modified Ashworth Scale (MAS: 0, 1, 1+, 2, 3, 4), which rates resistance to passive, brisk stretch[56]. Muscle groups examined included upper-limb flexor/adductor patterns (e.g., elbow flexors, wrist/finger flexors) and lower-limb adductors, knee extensors/flexors, and ankle plantarflexors. Testing followed a standardised procedure (relaxed

positioning, one slow familiarisation movement, then brisk stretch through the opposite direction of muscle action). For modelling, we derived a single patient-level binary endpoint: spasticity present if any paretic muscle scored MAS ≥1 (otherwise absent). MAS was not obtained by telephone; only in-person ratings were accepted.

All ratings were performed by clinicians trained in the respective instruments under written standard operating procedures. Definitions, time windows, and cut-offs were fixed a priori to ensure consistency between clinical measures and the imaging-based biomarkers analysed in this study.

3.3 Imaging acquisition and lesion masks

Clinical neuroimaging was obtained in the subacute window (day 3 –15) after stroke onset as part of routine care, using either non-contrast CT or MRI according to clinical indication. For MRI, sequences typically included T1-weighted, T2/FLAIR (for ischaemic lesions), and—when available—T2* or susceptibility-weighted imaging. Source DICOMs were exported to NIfTI format for processing. All imaging used for disconnectome analyses derived from this subacute study; no patient-specific diffusion tractography was required.

For MRI, volumes were bias-field corrected (N4) and brain-extracted; sequences from the same session were rigidly coregistered to a common reference (T1 or FLAIR). For CT, brain extraction and intensity windowing were applied as appropriate, and the CT was rigidly aligned to the AC–PC axis. Each subject's reference image (MRI or CT) was registered to the MNI152 1 mm template (https://nist.mni.mcgill.ca/icbm-152-nonlinear-atlases-2009/) via affine transformation followed by non-linear warping, using cost-function masking to avoid lesion-driven misregistration. The resulting transforms were applied to the lesion masks with nearest-neighbour interpolation. Left–right orientation and anatomical correspondence were verified systematically.

Lesions were manually segmented on the subacute scan that provided the best lesion–normal tissue contrast (FLAIR/T2 for ischaemia; CT or T2*/SWI for haemorrhage), by a trained rater from Physical and Rehabilitation Medicine and reviewed by a senior radiologist clinician; disagreements were resolved by consensus. Masks were saved as binary NIfTI volumes in native space and then propagated to MNI space using the transforms above[57].

A two-step quality control was performed: (i) visual inspection of native-space masks overlaid on the reference image in three orthogonal planes; (ii) verification after MNI normalisation to confirm correct placement relative to cortical and deep-white-matter landmarks and to exclude leakage into CSF or extra-cranial space. Cases with motion or artefacts precluding reliable segmentation/normalisation were excluded per protocol.

3.4 Advanced imaging lesion properties: local measures

To comprehensively characterize the three-dimensional morphological properties of acute ischemic lesions, the following local measures of lesion shape were computed using a standardized processing pipeline implemented within the in-house software, as previously described by Cheng et al.[58].

Following segmentation, each identified lesion was reconstructed in three-dimensional space, enabling a comprehensive analysis of its morphology. This reconstruction accounts for all lesion components, even if spatially discontinuous. From these 3D reconstructions, the following specific morphological descriptors were calculated:

- **Lesion Volume:** The total volume of the acute ischemic lesion, calculated in cubic millimeters (mm^3).
- **Lesion Surface Area:** The total surface area of the lesion, expressed in square millimeters (mm^2).

- **Oriented Minimum Bounding Box Volume (mm3):** This metric represents the volume of the smallest rectangular box that encloses all lesion components. Critically, its orientation is optimized to the lesion's principal axes, rendering it independent of the image coordinate system. This provides a robust measure of the spatial extent occupied by the lesion, accounting for its overall distribution and spread, including instances of multiple or fragmented lesion components.
- **Ratio of Bounding Box to Lesion Volume (Ratio_bb/lesion):** This dimensionless ratio quantifies the efficiency with which the bounding box volume is filled by the actual lesion. Lower values indicate more compact and spatially coherent lesions, while higher values suggest more irregular, scattered, or multifocal lesions, or those with significant internal cavitation.
- **Normalized Shape Factor (Lesion Sphericity):** This index describes the degree to which the lesion's shape approximates that of a perfect sphere. It is mathematically defined as

  $$S=(\sqrt{A}/V)/2.199085233$$

  where A denotes the lesion surface area and V represents the lesion volume. A value of 1.0 corresponds to a perfect sphere, with values increasing as the lesion's shape deviates further from an ideal spherical form, indicating greater irregularity or elongation.

This detailed, quantitative approach enabled us to move beyond qualitative visual assessments and simple volumetric estimations, providing objective insights into the complex three-dimensional architecture of acute stroke lesions.

3.5 Advanced imaging lesion properties: network measures

To move beyond lesion size and location, we quantified lesion-induced structural disconnection using the Network Modification (NeMo) framework[59] (https://kuceyeski-wcm-web.s3.amazonaws.com/upload.html). Each patient's lesion mask was overlaid on a normative

tractography connectome derived from healthy controls. For every pair of atlas regions, NeMo estimates the proportion of normative streamlines expected to be interrupted by the lesion. The resulting values are expressed as percent connectivity loss (0% = no loss; higher values = greater loss), and can be summarised at the edge, node, and whole-network levels.

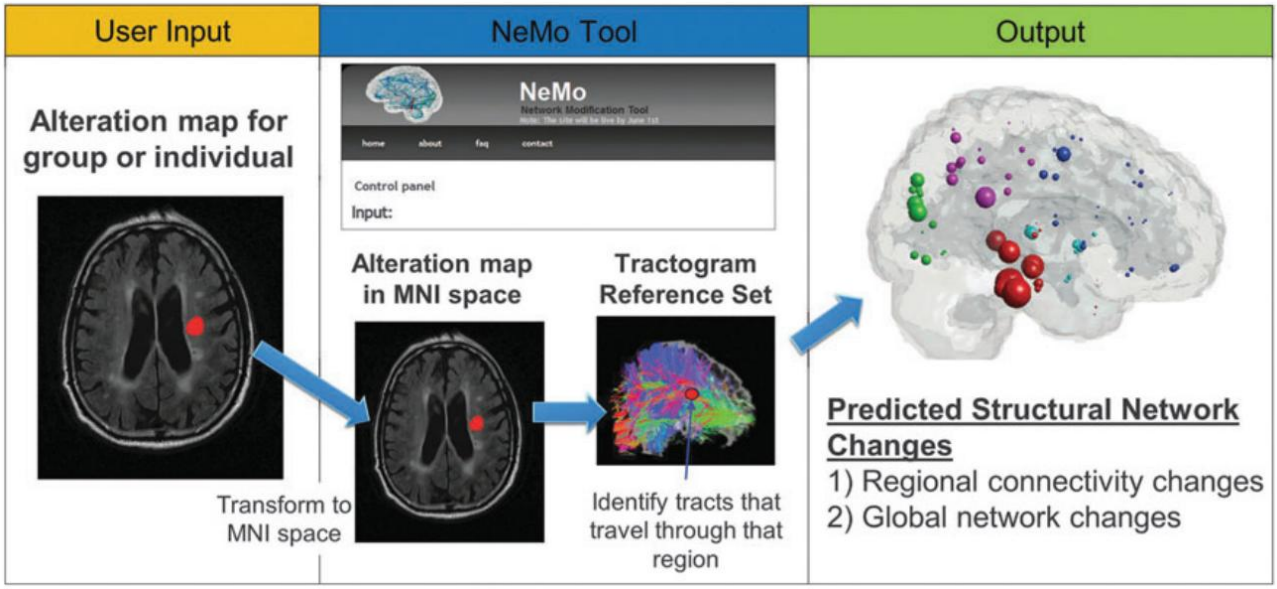

Figure 2 - The Network Modification (NeMo) tool workflow[60].

We used two complementary parcellations to ensure both network-level interpretability and regional specificity:

- Yeo 7-network framework [61]: the cortical mantle was organised according to the canonical 7-network taxonomy (Somatomotor, Visual, Dorsal Attention, Ventral/Salience, Frontoparietal Control, Default Mode, Limbic). This scaffold was used to aggregate edge-wise percent losses into interpretable within-system and between-system summaries. Hemisphere tags (left/right) were retained to isolate inter-hemispheric motor connections.
- Schaefer et al. (2018) functional atlas[62]: A cortico-subcortical parcellation with 443 regions provided sufficient nodal granularity to expose primary motor (precentral, M1) and supplementary motor (paracentral, SMA proxy) territories bilaterally, alongside sensory

cortices and deep nuclei (e.g., thalamus). This atlas underpinned nodal percent-loss metrics and their bilateral averages.

As demonstrated by Schaefer and colleagues in their original work[62], the boundaries of their parcels align closely with the boundaries of the seven canonical resting-state networks. This ensures that the large-scale network structure is preserved across different parcellation resolutions, allowing for a robust and coherent analysis at both the granular (parcel-level) and the system (network-level) scales.

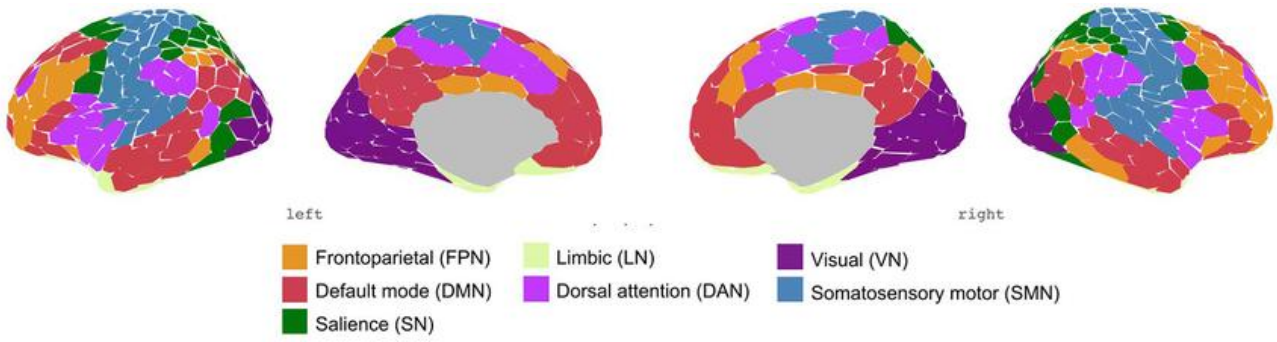

Figure 3 – Network structure from Yeo is preserved in 400 area parcellation from Schaefer atlas.

All masks and labels were verified for anatomical plausibility (hemisphere assignment, cortical network membership, subcortical boundaries) after spatial normalisation.

From this framework, a comprehensive set of metrics was derived to characterize the structural disconnectome at multiple topological scales:

- Global Network Disruption: A single metric, the percentage loss in Global Efficiency, was calculated to quantify the overall reduction in the brain's capacity for parallel information transfer as a result of the lesion.

- Network-Level Disconnection: We quantified the disconnection both within and between key functional systems. This included:
    - Within-Somatomotor Network Disconnection: The percentage of structural connections internal to the somatomotor network that were severed by the lesion.
    - Inter-Hemispheric Motor Disconnection: The percentage of connections between the homologous motor regions of the two hemispheres that were disrupted.
    - Motor to Associative Network Disconnection: The percentage of pathways connecting the motor system to the union of the Fronto-Parietal and Dorsal Attention networks that were damaged.
- Nodal Disconnection: At a more granular level, we calculated the percentage of structural disconnection for five key sensorimotor nodes: the primary motor cortex (M1), the primary somatosensory cortex (S1), the supplementary motor area (SMA), the premotor dorsal cortex (PMd), and the thalamus.
- Composite and Laterality Indices: To synthesize this information and assess asymmetry, several derived indices were computed:
    - The Motor Network Disconnection Index (MNDI), a composite score integrating the disconnection of M1 and SMA.
    - The Motor Network Disconnection Index 3 (MNDI3), focusing on M1, SMA, and PMd.
    - Laterality Indices for M1 and SMA, calculated to quantify the degree of asymmetry in disconnection between the ipsilesional and contralesional nodes.

3.6 Statistical analysis

All statistical analyses were performed using Python (scikit-learn, pandas, matplotlib)[63]. Given the limited sample size and event-per-variable constraints, we pre-specified parsimonious models with a maximum of three predictors, in line with established recommendations for prediction modeling[64] .

For binary outcomes (mRS and FAC improvement, and spasticity), we applied logistic regression with L2 penalization, which has been shown to reduce overfitting and improve generalizability in small datasets [65]. For the continuous outcome (NIHSS motor score at 12 months), ridge regression was used to stabilize coefficient estimates under multicollinearity and low subject-to-variable ratios [6]. All continuous predictors were standardized (z-scores) prior to modeling, and effect sizes were expressed as odds ratios (OR) per interquartile range (IQR) for logistic models and β per IQR for ridge regression, a strategy recommended for clinical interpretability of scaled predictors[65,66]. Internal validation was performed using stratified 5-fold cross-validation for binary outcomes and leave-one-out cross-validation (LOOCV) for the continuous outcome, methods widely endorsed to reduce optimism bias in small samples. Model performance was assessed using area under the ROC curve (AUC), Brier score, and calibration plots for logistic regression, and with R^2, root mean squared error (RMSE), and mean absolute error (MAE) for ridge regression. To quantify uncertainty, bootstrap resampling with 50 iterations was performed to derive confidence intervals for predictive performance[67]. The reporting of model development and validation followed the TRIPOD (Transparent Reporting of a multivariable prediction model for Individual Prognosis Or Diagnosis) guidelines.

CHAPTER 4 - RESULTS

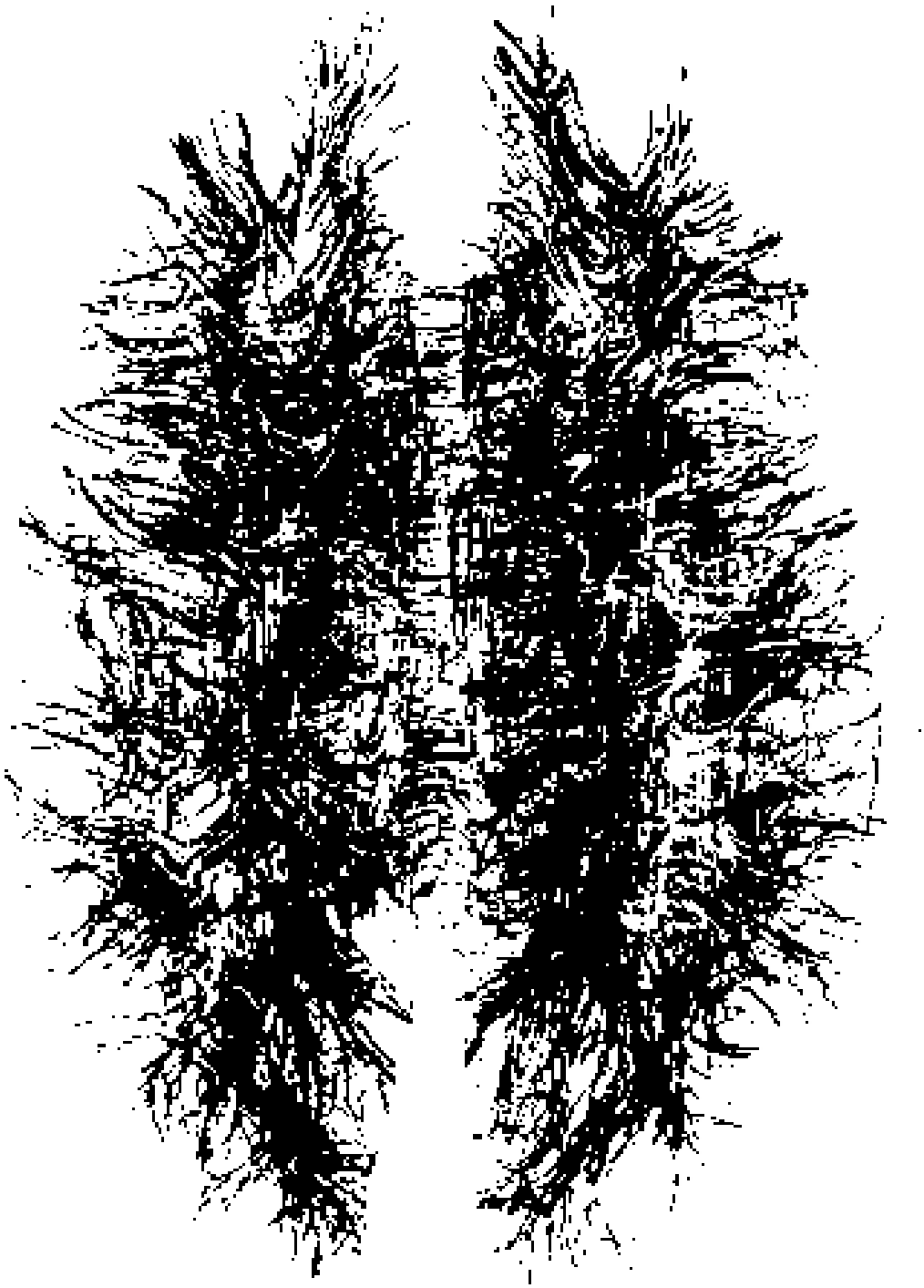

4.1 Participants

A total of 31 patients with acute stroke were initially recruited for this study. Of this cohort, two patients were subsequently excluded from longitudinal analysis due to imaging artifacts that precluded accurate lesion segmentation, and one lost to follow-up at the 12-month timepoint (one due to mortality). This resulted in a final cohort of 28 patients with complete baseline imaging, clinical data, and 12-month functional outcomes available for the primary analyses. The baseline demographic and clinical characteristics of the final cohort are summarized in table 1.

Table 1: Baseline Demographic and Clinical Characteristics of the Patient Cohort (N=28)

Characteristic	Value
Age (years), Mean (SD)	64.1 (10.9)
Sex, n (%)	
Male	17 (60.7%)
Female	11 (39.3%)
Stroke Type, n (%)	
Ischemic	20 (71.4%)
Intracerebral Hemorrhage (ICH)	8 (28.6%)
Lesion Side, n (%)	
Right Hemisphere	18 (64.3%)
Left Hemisphere	10 (35.7%)
Imaging Modality, n (%)	
Computed Tomography (CT)	18 (64.3%)
Magnetic Resonance Imaging (MRI)	10 (35.7%)
NIHSS Total Score, Mean (SD)	10.7 (4.8)
NIHSS Motor Score, Mean (SD)	5.5 (2.5)

The mean age of the patients was 64.1 ± 10.9 years, and the cohort comprised 17 males (60.7%) and 11 females (39.3%). The cohort was predominantly composed of patients with ischemic stroke (n=20, 71.4%), with the remainder having experienced intracerebral hemorrhage (n=8, 28.6%). Lesions were more frequently located in the right hemisphere (n=18, 64.3%) than the left (n=10, 35.7%). At the time of admission (T0), the median stroke severity was moderate, with a mean total National Institutes of Health Stroke Scale (NIHSS) score of 10.7 ± 4.8. The motor-specific subscore of the NIHSS had

a mean of 5.5 ± 2.5. Baseline neuroimaging was performed using either non-contrast CT (n=18, 64.3%) or MRI (n=10, 35.7%) for initial lesion identification.

4.2 Lesion characterization and network-level disconnectome

Lesions within the patient cohort were predominantly supratentorial (n=26, 92.9%), with two cases involving subtentorial structures. A right hemispheric predominance was observed (n=18, 64.3%). Anatomical review indicated frequent involvement of deep white matter and subcortical structures, including the corona radiata and internal capsule, consistent with the cohort's clinical presentation of motor deficits.

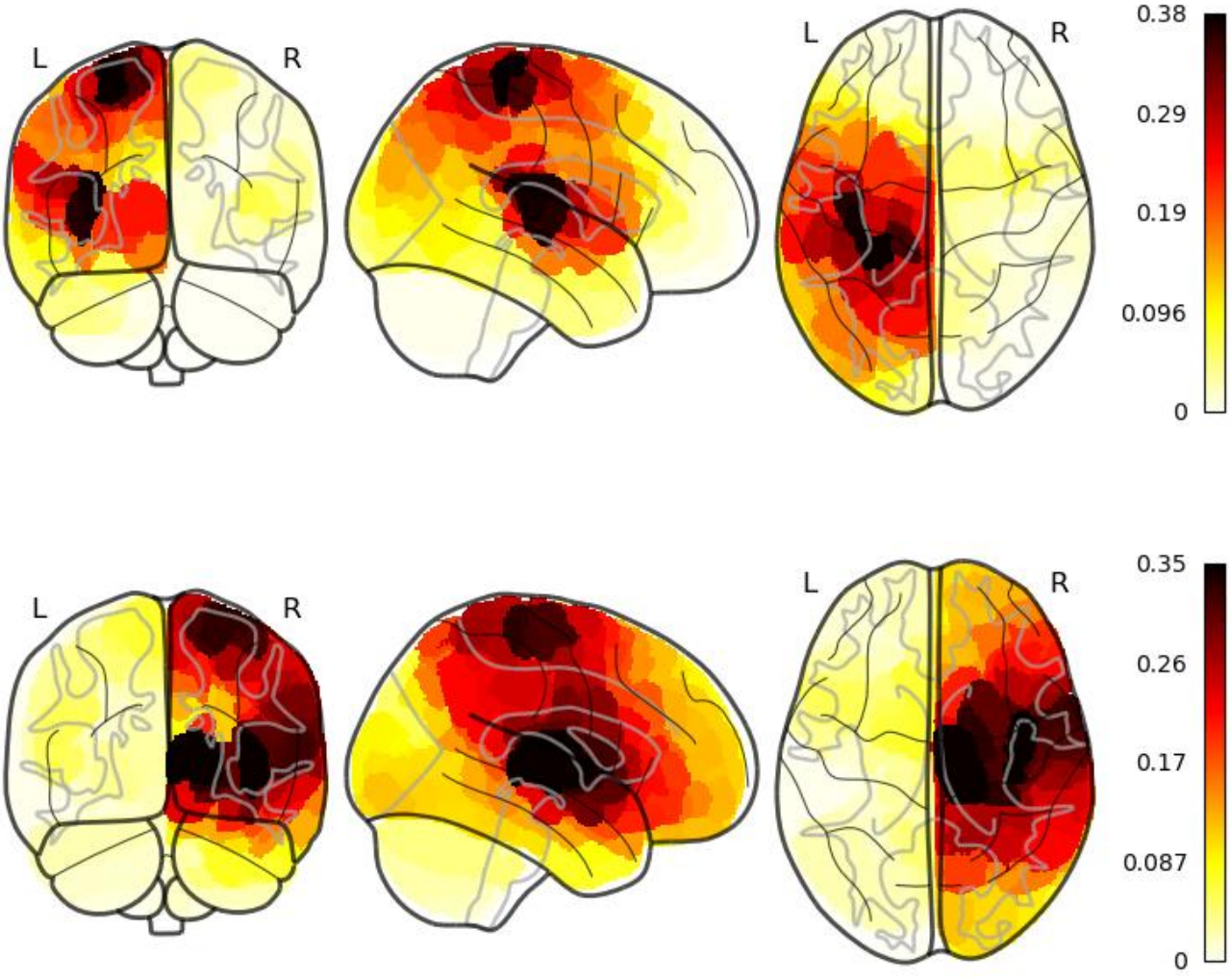

Figure 4 -Lesion map of total sample: left hemisphere (Top) and right hemisphere (Bottom)

Lesion volume was highly variable and exhibited a non-normal distribution, with a median of 9,121 mm^3 (IQR: 3,698 – 35,275 mm^3). Beyond simple volume, lesions displayed considerable geometric complexity and irregularity. The median lesion sphericity was 0.68 (IQR: 0.57 – 0.75), a value that indicates a consistent deviation from a compact, spherical morphology. This geometric irregularity was further quantified by the ratio of the lesion's bounding box to its true volume, a measure of spatial dispersion. This ratio had a median of 3.40 (IQR: 3.08 – 4.49), signifying that lesions were often spatially dispersed and elongated rather than being focal and contained.

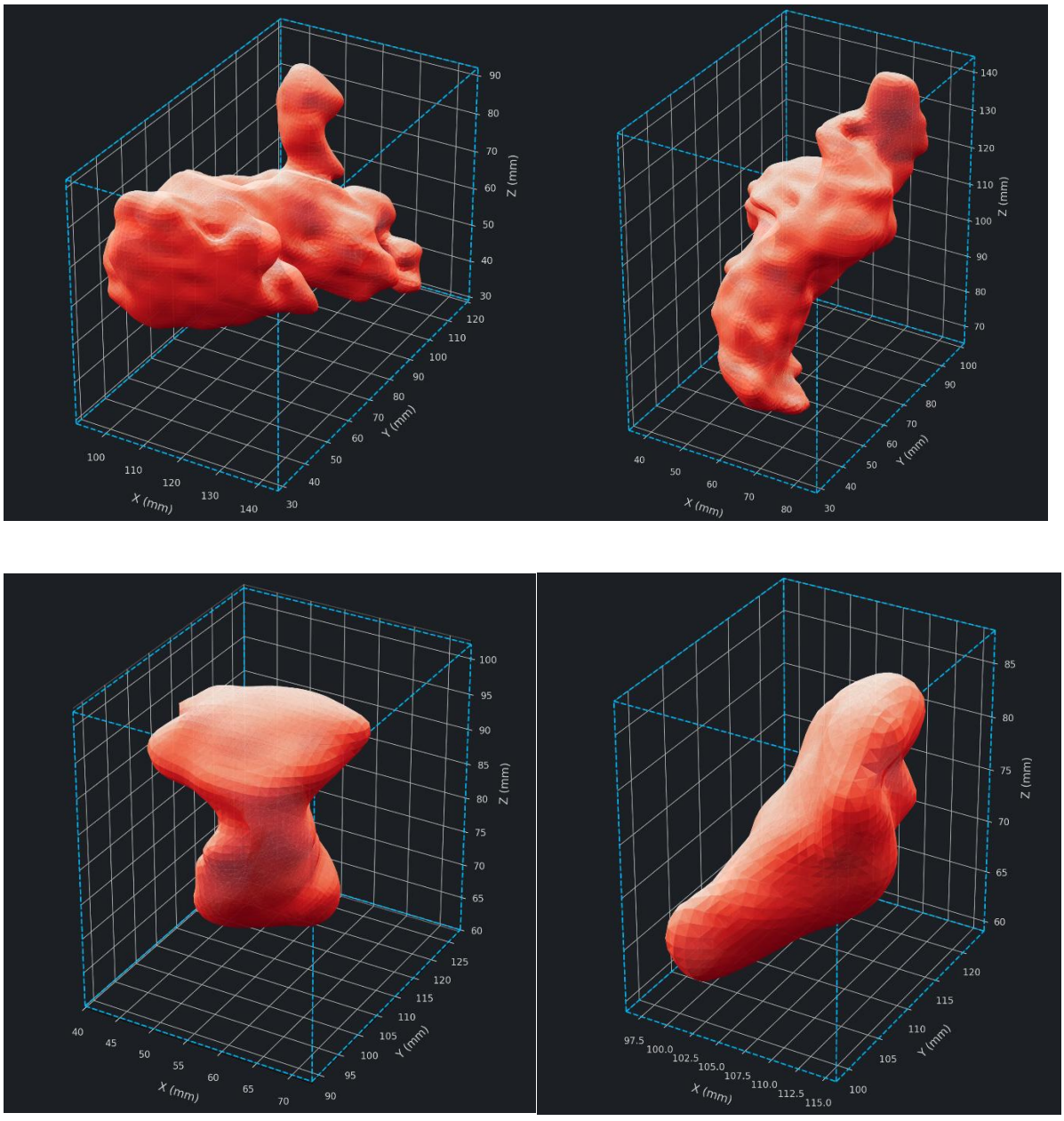

Figure 5 – Examples of four different 3D lesion from patients.

At a global network level, the structural disconnectome induced by these lesions resulted in a modest but consistent reduction in overall network efficiency, with a median loss of 0.15% (IQR: 0.08% – 0.26%). However, this subtle global effect masked more profound and functionally relevant disruptions within and between specific subnetworks. Analysis at the nodal level revealed the severe impact on the core sensorimotor system. The median disconnection of pathways associated with the primary motor cortex (M1) was 25.0% (IQR: 19.8% – 34.4%), and was similarly high for the primary somatosensory cortex (S1) (median 22.9%; IQR: 18.2% – 33.2%). Key motor planning regions were also heavily affected, including the supplementary motor area (SMA) (median 21.0%; IQR: 17.2% – 28.8%) and the premotor dorsal cortex (PMd) (median 17.3%; IQR: 15.2% – 28.0%). Critically, disconnection extended to the subcortical level, with a median thalamic disconnection of 27.2% (IQR: 18.0% – 50.0%).

To synthesize these nodal disruptions, two composite scores were calculated. The comprehensive Motor Network Disconnection Index (MNDI) had a median value of 0.234 [IQR: 0.188 – 0.273] and the three-node variant (MNDI3) showed a similar distribution, with a median value of 0.241 [IQR: 0.190 – 0.292].

The broader topological "fingerprint" of disconnection across the seven canonical Yeo networks revealed a clear pattern of vulnerability. As expected, the Somatomotor Network (SMN) sustained the most severe internal disruption. However, significant disconnection was also observed within associative networks, particularly the Dorsal Attention and Control Networks. In contrast, the Limbic Network was relatively spared across the cohort, indicating a specific, non-uniform pattern of network damage driven by the typical vascular territories affected by stroke.

Table 2 summarized all the variables.

Table 2: Lesion Geometry and Structural Connectome Disruption Metrics

Metric	Median [IQR]
Lesion Geometry	
Lesion Volume (mm^3)	9121 [3698 – 35275]
Lesion Surface (mm^2)	3040 [1558 – 11763]
Lesion Sphericity	0.68 [0.57 – 0.75]
Spatial Dispersion (Bounding Box / Lesion Volume Ratio)	3.40 [3.08 – 4.49]
Global and Network-Level Disconnection	
Global Efficiency Loss (%)	0.15 [0.08 – 0.26]
Within-Somatomotor Network Disconnection (%)	0.07 [0.04 – 0.17]
Inter-Hemispheric Motor Disconnection (%)	0.09 [0.04 – 0.22]
Motor to FPN/DA Disconnection (%)	0.08 [0.05 – 0.11]
Nodal Disconnection (Motor System)	
Primary Motor Cortex (M1) Disconnection (%)	25.0 [19.8 – 34.4]
Primary Somatosensory Cortex (S1) Disconnection (%)	22.9 [18.2 – 33.2]
Supplementary Motor Area (SMA) Disconnection (%)	21.0 [17.2 – 28.8]
Premotor Dorsal Cortex (PMd) Disconnection (%)	17.3 [15.2 – 28.0]
Thalamus Disconnection (%)	27.2 [18.0 – 50.0]
Composite Score	
Motor Network Disconnection Index (MNDI)	0.23 [0.18 – 0.29]
Motor Network Disconnection Index 3 (MNDI)	0.24 [0.19 – 0.29]
Within-Network Disconnection (Yeo-7 Networks)	
Somatomotor Network Loss (%)	0.07 [0.04 – 0.17]
Dorsal Attention Network Loss (%)	0.05 [0.02 – 0.10]
Salience/Ventral Attention Network Loss (%)	0.05 [0.02 – 0.10]
Control Network Loss (%)	0.07 [0.05 – 0.10]
Default Mode Network Loss (%)	0.04 [0.02 – 0.07]
Visual Network Loss (%)	0.03 [0.01 – 0.13]
Limbic Network Loss (%)	0.02 [0.01 – 0.04]

Abbreviations: IQR, Interquartile Range; FPN, Fronto-Parietal Network; DA, Dorsal Attention Network; MNDI, Motor Network Disconnection Index.

4.3 Twelve-month clinical outcomes

At the 12-month follow-up, clinical outcomes for the entire cohort of 28 patients were assessed. Functional independence, defined as a modified Rankin Scale (mRS) score of ≤2, was achieved by 13 of the 28 patients (46.4%; 95% CI [27.5% – 66.1%]). Ambulatory independence, defined by a Functional Ambulation Classification (FAC) score of ≥4, was observed in 17 of the 28 patients

(60.7%; 95% CI [40.6% – 78.5%]). The prevalence of post-stroke spasticity, defined as a score of ≥1 on the Modified Ashworth Scale in any tested muscle group, was present in 12 of the 28 patients (42.9%; 95% CI [24.5% – 62.8%]) at the one-year timepoint.

Motor recovery was quantified by the change in the NIHSS motor subscore from baseline to 12 months (ΔNIHSS-motor). The cohort demonstrated a median improvement of -2.0 points [IQR: -3.0 to -1.5], where negative values signify clinical improvement. This indicates that while half of the patients experienced a motor score improvement of at least 2 points, the overall degree of motor recovery was highly variable across the cohort.

4.4 Bivariate associations between early disconnectome and outcomes

Unadjusted bivariate associations were examined between prespecified baseline imaging metrics and 12-month clinical outcomes. For binary outcomes, group contrasts were assessed using the Mann-Whitney U test, with the False Discovery Rate (FDR) applied to control for multiple comparisons across the family of tests for each outcome.

4.4.1 Functional Independence (mRS ≤ 2)

The analysis revealed a significant association between global network disruption and functional independence at 12 months. Patients who did not achieve functional independence (mRS > 2; n=15) had a significantly lower median loss in global efficiency compared to those who did achieve independence (mRS ≤ 2; n=13) (Median ΔGlobalEfficiency: 0.001134 vs. 0.002605; Mann-Whitney U = 39, p = 0.008, q = [q-value]). A trend-level association was also observed for the disconnection of the supplementary motor area, where patients with a poorer outcome tended to have higher SMA disconnection (SMA_Pair_WithinStrength_Delta: 0.243583 vs. 0.176231; Mann-Whitney U = 136, p = 0.080, q = [q-value]). No other prespecified metrics, including the composite MNDI3 score, showed a significant association with functional independence at the bivariate level. Patients who

achieved functional independence (mRS ≤ 2; n=13) had lower baseline severity (NIHSS_T0_Motor median 4.0 vs 8.0, $p = 1.29\times10^{-5}$) and smaller lesions (5,332 vs 31,320 mm^3, p = 0.024).

4.4.2 Ambulatory Independence (FAC ≥ 4)

Patients who achieved ambulatory independence showed less SMA asymmetry (SMA laterality index median −0.071 vs −0.376, p = 0.0048) and lower baseline severity (NIHSS_T0_Motor 4.0 vs 7.0, p = 0.0039). No other significant associations were found between any of the prespecified disconnectome or lesion metrics and the achievement of ambulatory independence at 12 months. All unadjusted p-values were greater than 0.25, indicating no discernible group differences in the underlying network disruption metrics between patients who were able to walk independently and those who were not.

4.4.3 Spasticity

At the 12-month timepoint, no prespecified imaging metric was significantly associated with the presence of spasticity (MAS ≥ 1). Spastic patients had higher baseline severity (NIHSS_T0_Motor 7.5 vs 4.0, p = 0.0016). All bivariate comparisons yielded non-significant results, with the lowest unadjusted p-value being 0.13 for the loss in global efficiency. Differences for Within-motor disconnection (median 5.84×10^{-4} vs 5.13×10^{-4}) and SensoryIndex (median 0.207 vs 0.246) did not reach significance (both p ≈ 0.34).

4.5 Predictive Models

A series of predictive models was developed for four primary 12-month clinical outcomes, utilizing baseline clinical data, lesion metrics, and disconnectome-derived indices. A total of 28 patients were included in these analyses. A consistent finding across all outcomes was that models combining acute clinical severity (NIHSS T0 Motor) with disconnectome or lesion metrics consistently outperformed specifications based solely on imaging data, although the latter retained useful predictive information.

4.5.1 Prediction of Functional Independence (mRS Improvement)

The prediction of functional independence at 12 months (defined as mRS ≤ 2) was robustly informed by both lesion geometry and disconnectome metrics. In the univariate analysis, Lesion Sphericity emerged as the most powerful single imaging predictor, demonstrating excellent discriminatory capacity with a cross-validated Area Under the Curve (AUC CV) of 0.785. This was closely followed by ΔGlobal Efficiency (AUC CV = 0.774) and the Ratio of Bounding Box to Lesion Volume (AUC CV = 0.754), underscoring the profound importance of both the geometric irregularity and the global network impact of the lesion. Other metrics, including lesion volume and surface area, also showed good univariate performance, while nodal disconnection indices like MNDI3 had more moderate predictive power on their own (Figure 6).

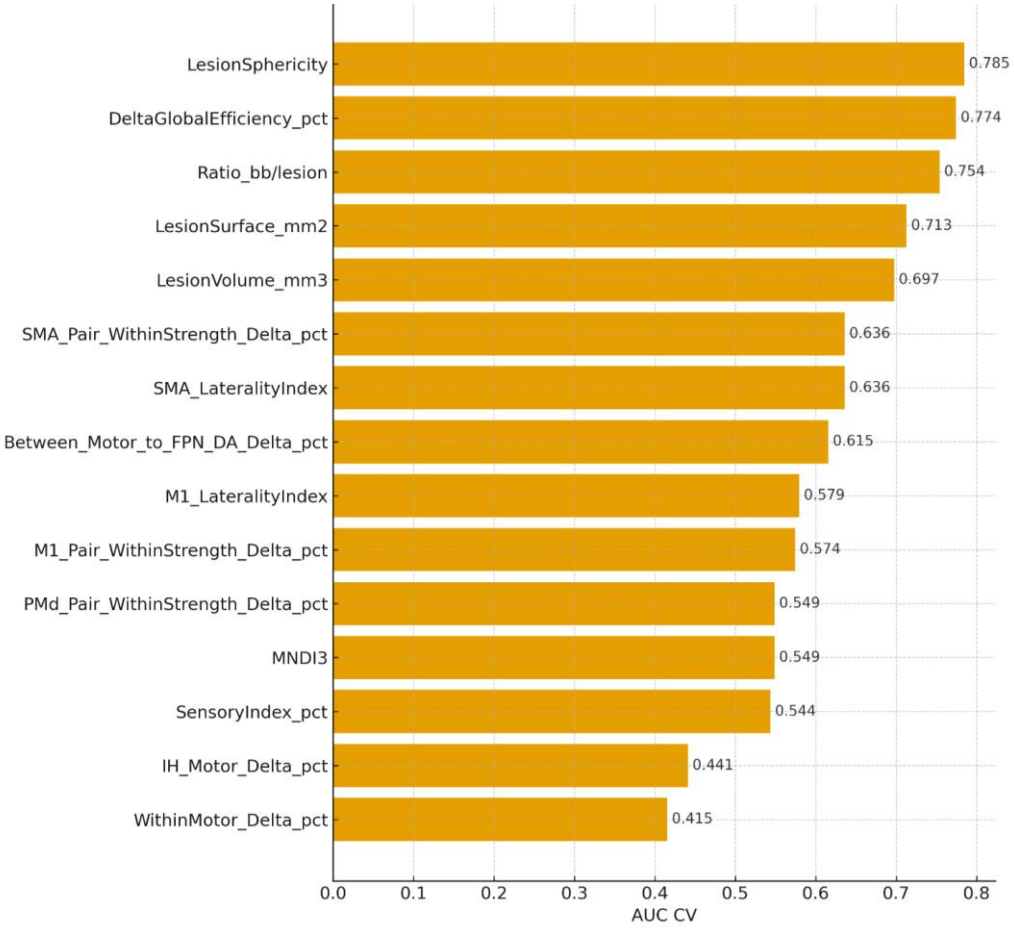

Figure 6 - Top 15 predictors of functional improvement (mRS) based on univariate analysis

Multivariate modeling significantly enhanced predictive accuracy. The optimal model integrated baseline motor severity (NIHSS_T0_Motor) with Lesion Sphericity and the composite disconnectome score MNDI3. This combined specification achieved outstanding discrimination, with a cross-validated AUC of 0.974. As illustrated by the ROC comparison, several other models combining clinical and imaging data also performed exceptionally well, including a model with Within-Motor disconnection and an SMA Laterality Index (AUC = 0.964) and another with lesion volume and MNDI3 (AUC = 0.954). Crucially, models based exclusively on imaging data retained significant predictive power; a specification combining Lesion Sphericity and ΔGlobal Efficiency yielded a strong AUC of 0.800, demonstrating that imaging can provide a robust prognosis even in the absence of clinical scores (Figures 7 and 8).

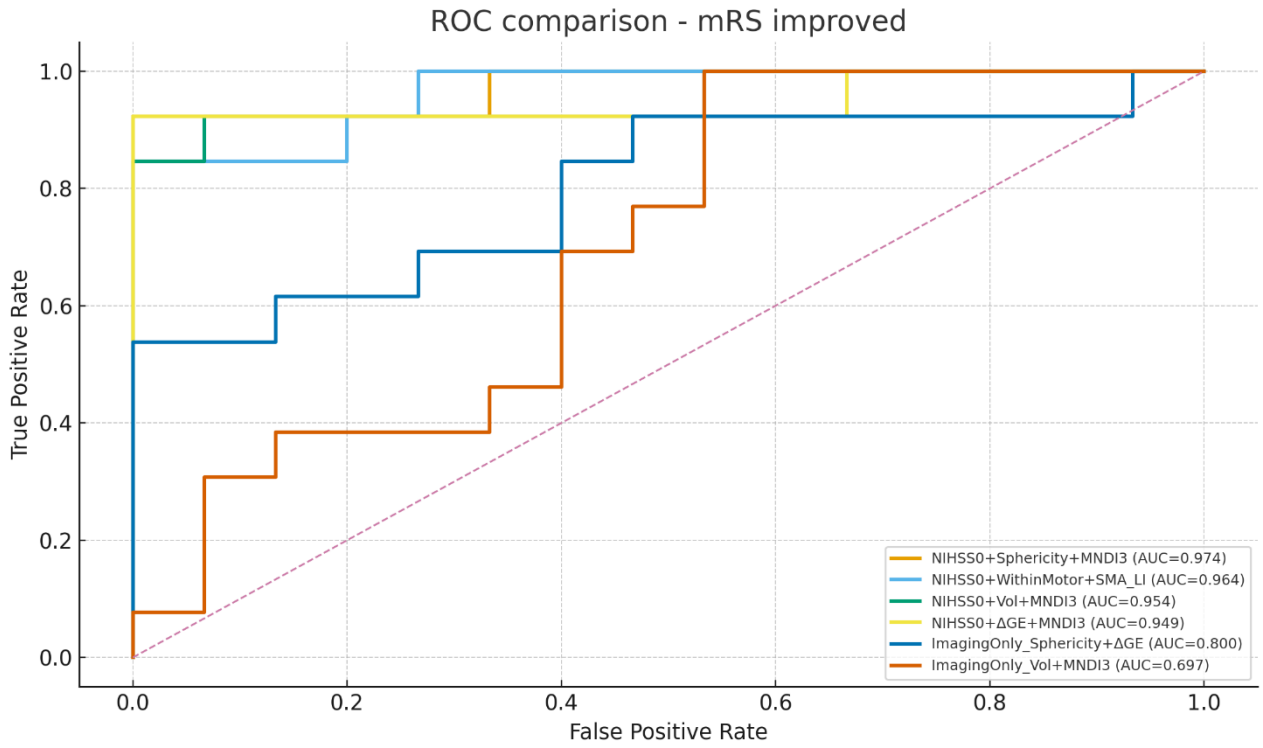

Figure 6 - ROC curve comparison for models predicting mRS improvement.

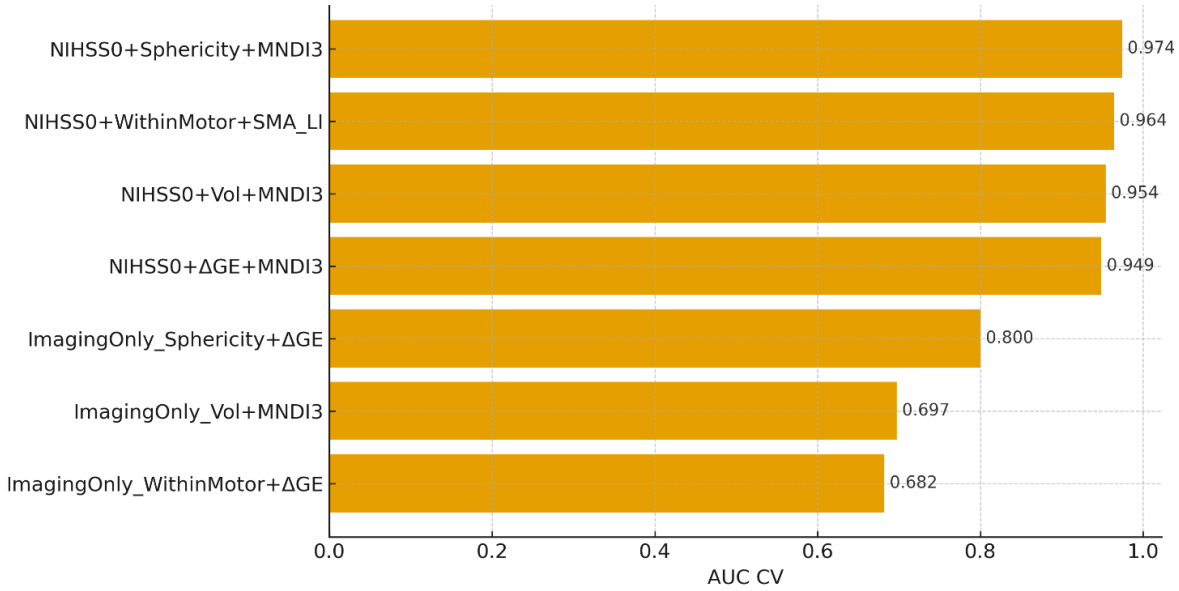

Figure 7 – Top Multivariate models predicting mRS improvement.

Analysis of the effect sizes within the top-performing multivariate model revealed the independent contributions of each variable. Lesion Sphericity was the most influential predictor, with an odds ratio (OR) per IQR of approximately 2.2, indicating that a more irregular, less spherical lesion more than doubles the odds of a poor functional outcome. The MNDI3 was the second most important factor (OR ≈ 1.25), confirming that greater disconnection of the core motor network independently predicts a lower likelihood of functional independence. In this multivariate context, the effect of baseline motor severity (NIHSS T0 Motor) was minimal, suggesting that its predictive information was largely captured by the more mechanistic measures of lesion geometry and network disruption.

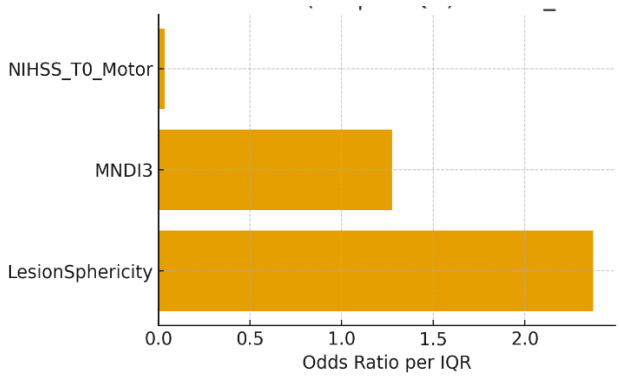

Figure 8 - Effect sizes for predictors of mRS improvement.

4.5.2 Prediction of Ambulatory Independence

The prediction of ambulatory independence at 12 months was strongly driven by metrics reflecting the asymmetry and global impact of network disconnection. In the univariate analysis, the SMA Laterality Index was the most powerful single predictor, demonstrating excellent discriminatory capacity with a cross-validated Area Under the Curve (AUC CV) of 0.791. This was followed by the M1 Laterality Index (AUC CV = 0.674) and the disconnection of the premotor dorsal cortex (PMd) (AUC CV = 0.604), highlighting the particular importance of the integrity and interhemispheric balance of higher-order motor planning areas for gait recovery. Global network disruption (ΔGlobal Efficiency) and the composite MNDI3 score also showed moderate univariate predictive power (Figure 9).

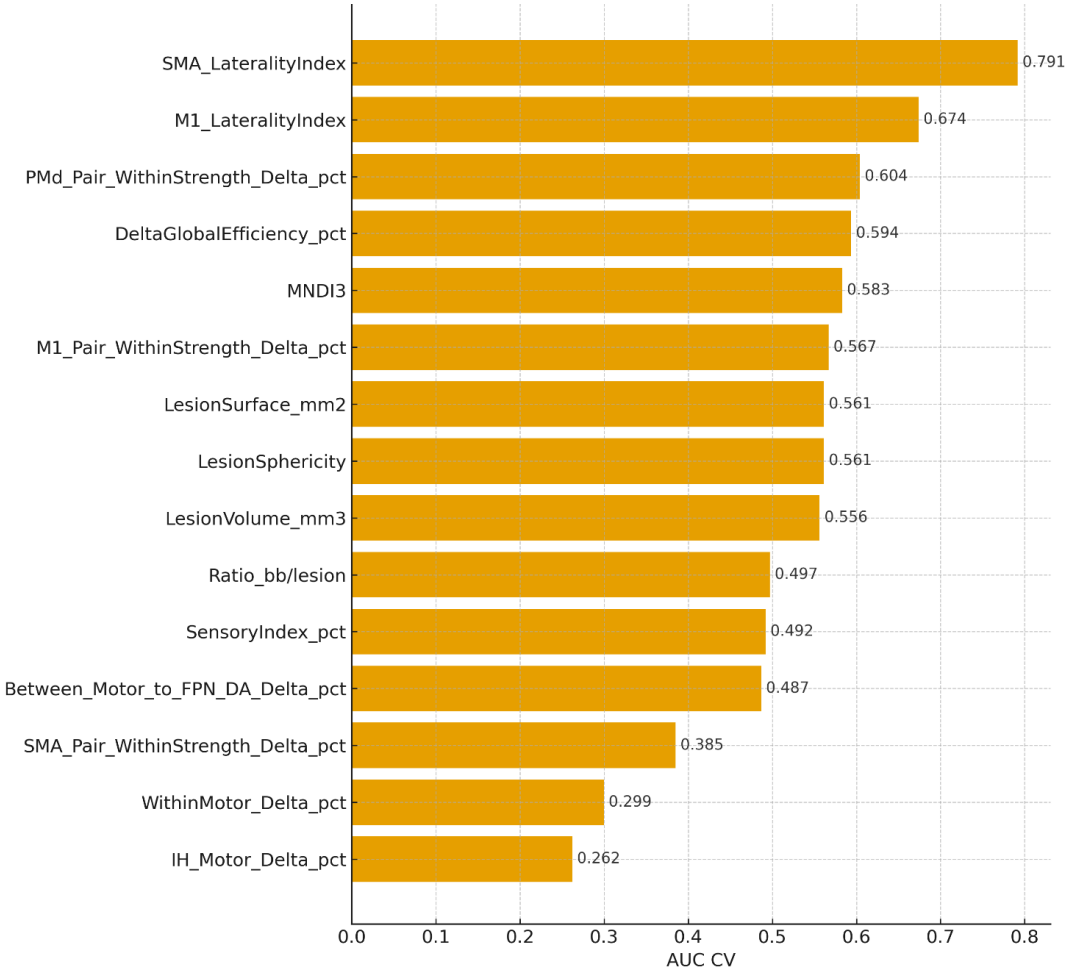

Figure 9 – Top 15 predictors of Ambulatory Independence based on univariate analysis.

Multivariate modeling further refined these associations and significantly improved predictive accuracy. The optimal model for ambulatory outcome integrated baseline motor severity (NIHSS_T0_Motor) with ΔGlobal Efficiency and the SMA Laterality Index. This combined specification achieved outstanding discrimination with a cross-validated AUC of 0.952. The ROC comparison illustrates that other models incorporating the SMA Laterality Index also performed exceptionally well, including a model with Within-Motor disconnection (AUC = 0.947) and another with the MNDI3 (AUC = 0.920). Notably, imaging-only models retained strong predictive value; a specification combining the SMA Laterality Index with lesion volume yielded a robust AUC of 0.829, underscoring the clinical utility of these metrics even without baseline clinical data (Figures 10 and 11).

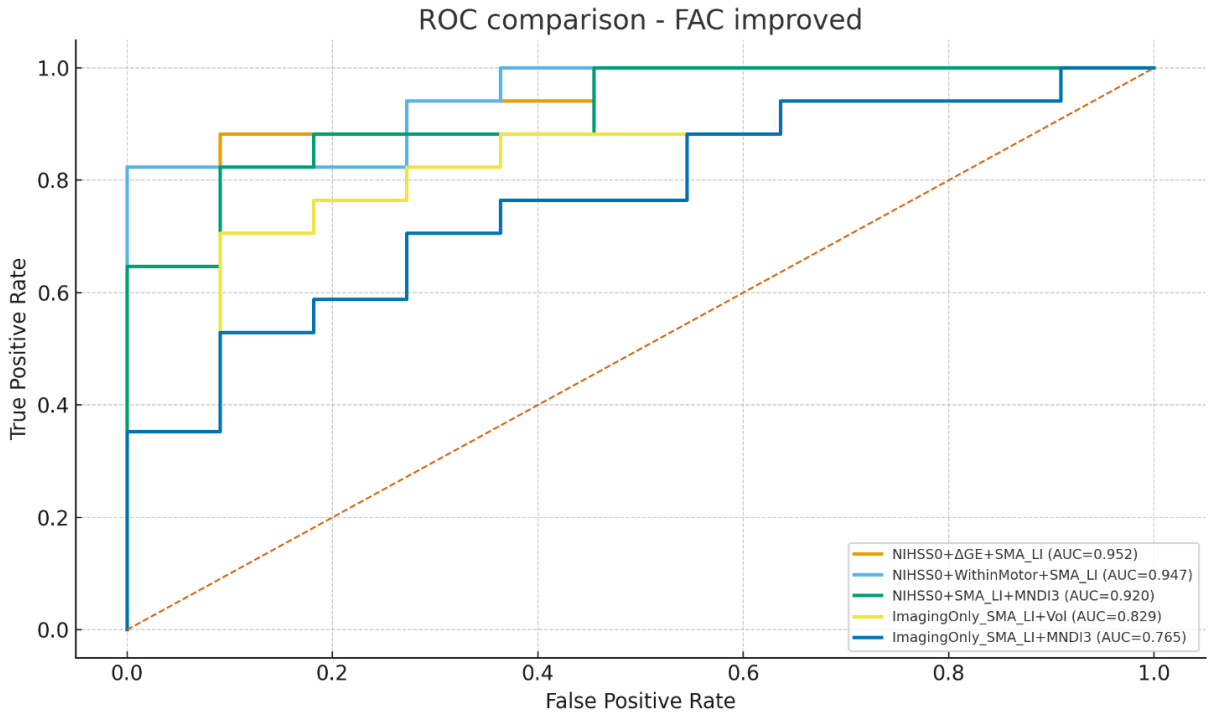

Figure 10 – ROC curve comparison for models predicting Ambulatory Independence

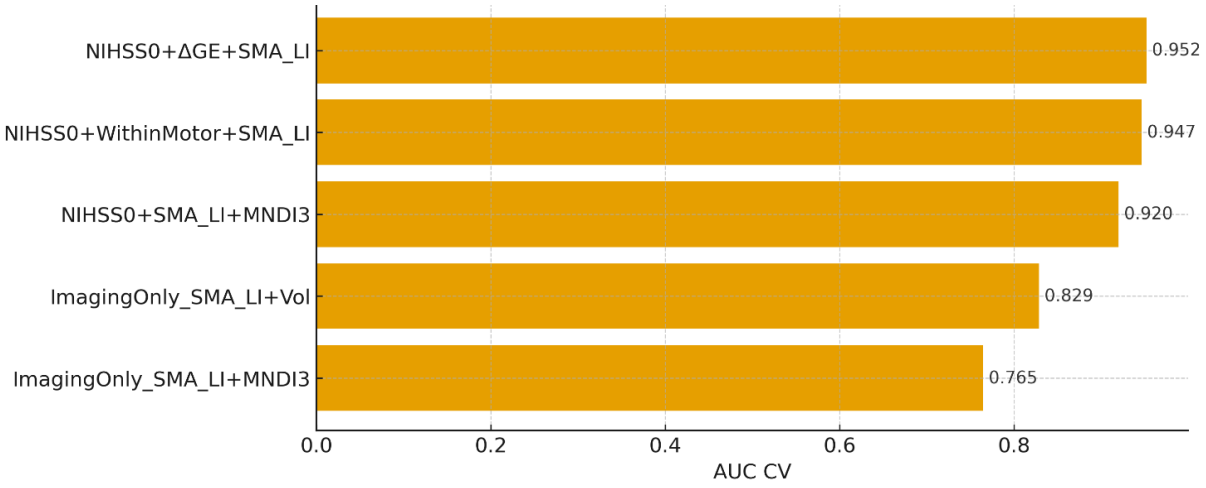

Figure 11 - Top Multivariate models predicting FAC improvement

Analysis of the effect sizes within the top-performing multivariate model confirmed the dominant role of network asymmetry. The SMA Laterality Index was by far the most influential predictor, with an odds ratio (OR) per IQR of approximately 6.2. This indicates that a greater imbalance in the disconnection of the supplementary motor areas dramatically increases the odds of a poor ambulatory outcome. ΔGlobal Efficiency was a significant secondary predictor (OR ≈ 1.7), suggesting that the overall efficiency of the surviving brain network also contributes independently to gait recovery. Similar to the models for functional independence, the effect of baseline motor severity was minimal in the multivariate context, reinforcing the conclusion that specific patterns of network disruption are more predictive of long-term ambulatory function than the initial motor deficit itself.

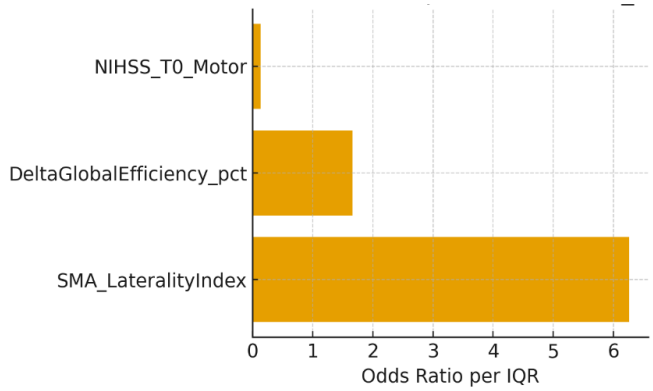

Figure 12 - Effect sizes for predictors of FAC improvement.

4.5.3 Prediction of Post-Stroke Spasticity

The prediction of spasticity at 12 months (MAS ≥ 1) was investigated through both univariate and multivariate models. In the univariate analysis, which assessed the individual predictive capacity of each imaging metric, the loss in global network efficiency (ΔGlobal Efficiency) emerged as the strongest single predictor, achieving a cross-validated Area Under the Curve (AUC CV) of 0.65. This was followed by the Sensory Index (AUC CV = 0.54) and the disconnection of pathways between the motor and frontoparietal/dorsal attention networks (AUC CV = 0.51). Notably, metrics directly related to the motor system, such as lesion volume and the MNDI3, demonstrated only weak to moderate univariate predictive power (Figure 13).

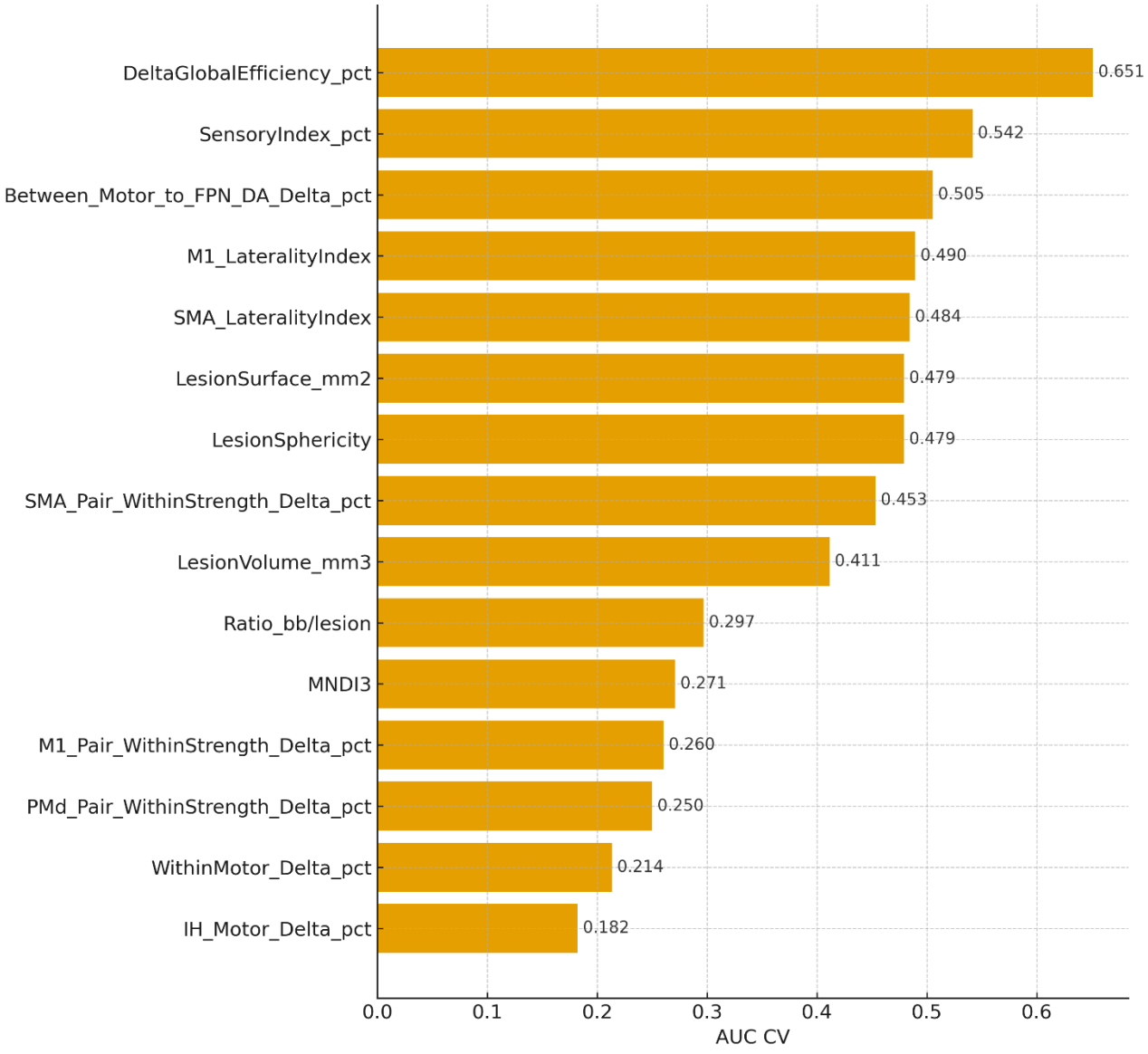

Figure 13 – Top 15 predictors of spasticity based on univariate analysis.

However, a substantially higher predictive accuracy was achieved through multivariate modeling. The strongest model combined baseline clinical severity (NIHSS_T0_Motor) with the degree of disconnection within the somatomotor network (WithinMotor_Delta_pct). This specification achieved robust discrimination with a cross-validated AUC of 0.771. An alternative model, substituting the disconnectome metric with lesion volume (NIHSS0+Vol), performed identically (AUC CV = 0.771), suggesting that in the presence of a strong clinical predictor, the specific contribution of different imaging metrics may be partially redundant. In contrast, models based solely on imaging predictors were substantially weaker; the best imaging-only model, combining ΔGlobal Efficiency and the Sensory Index, yielded a significantly lower AUC of 0.625 (Figures 14 and 15).

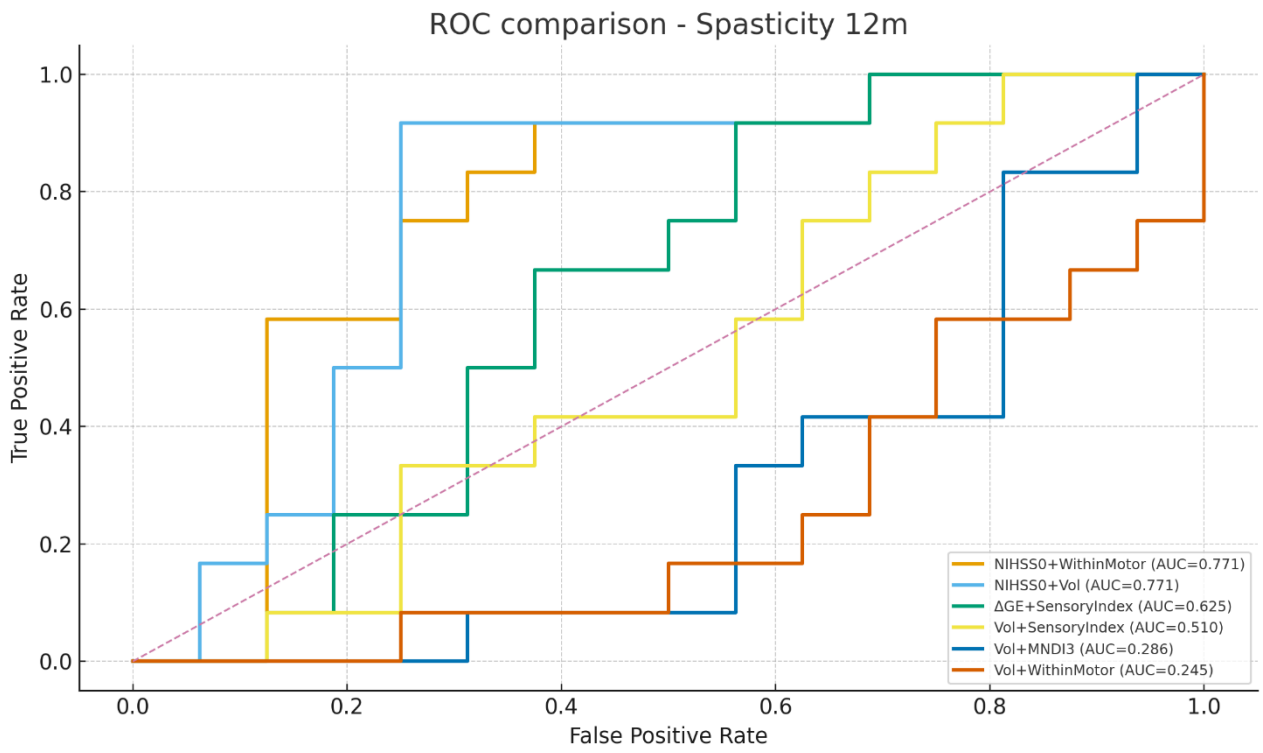

Figure 14 – ROC curve comparison for models predicting spasticity

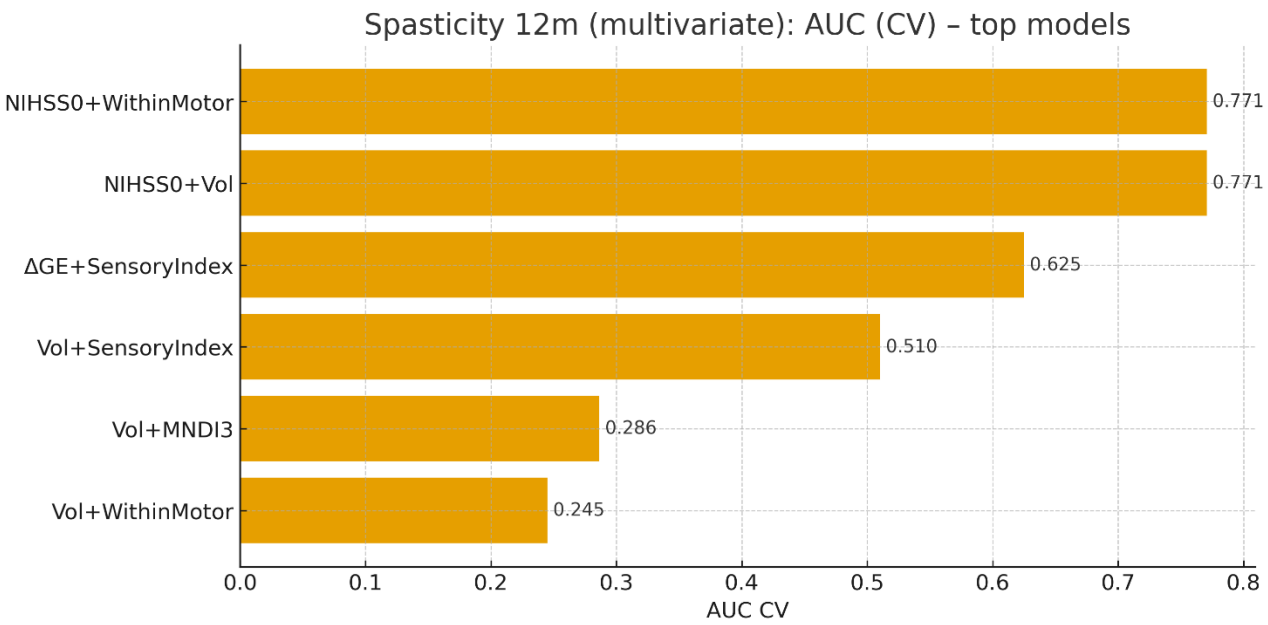

Figure 15 - Top Multivariate models predicting FAC improvement

Analysis of the effect sizes within the top-performing multivariate model confirmed the dominant role of the initial clinical deficit. Baseline motor severity was the overwhelmingly strongest predictor, with an odds ratio per IQR of approximately 9.0, indicating that a more severe initial motor impairment dramatically increases the likelihood of developing spasticity. The Within-Motor disconnection metric provided a smaller but independent contribution, with an odds ratio of approximately 1.1 per IQR. These findings consistently demonstrate that while structural disconnection within the motor system is a statistically relevant factor, the initial severity of the clinical motor insult remains the principal determinant of long-term post-stroke spasticity.

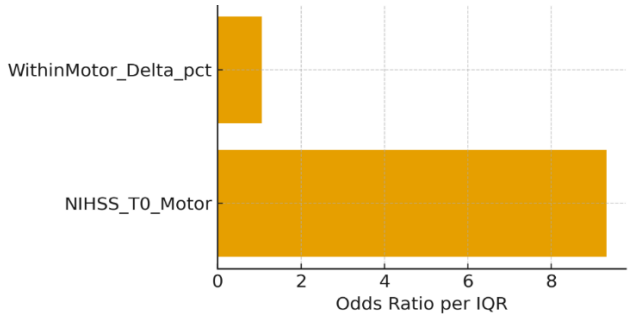

Figure 16- Effect sizes for predictors of spasticity.

4.5.4 Prediction of Continuous Motor Score

Finally, for the continuous outcome of the 12-month NIHSS motor score, a ridge regression approach was employed. The optimal model, which included baseline motor severity, lesion volume, and the MNDI3, explained a substantial portion of the variance in long-term motor outcomes ($R^2 = 0.66$, 95% CI [bootstrap]: 0.40–0.78, validated with Leave-One-Out Cross-Validation). The model's predictive accuracy was further supported by a low Root Mean Squared Error (RMSE) of approximately 2.1 points and a Mean Absolute Error (MAE) of approximately 1.5 points. In stark contrast, an imaging-only model using lesion volume and MNDI3 performed substantially less well, explaining only a small fraction of the variance ($R^2 \approx 0.22$). Within the full model, both larger lesion volume and greater nodal motor disconnection independently predicted a worse long-term motor deficit, even after accounting for the initial severity of impairment.

Outcome	Type	Measure	Performance
NIHSS motor (12m)	Clinical + Disconnectome	NIHSS_T0 + LesionVolume + MNDI3	R^2=0.658
NIHSS motor (12m)	Disconnectome	LesionVolume + MNDI3	R^2=0.216
mRS improved (12m)	Clinical + Disconnectome	NIHSS_T0 + LesionSphericity + MNDI3	AUC=0.974
mRS improved (12m)	Disconnectome	LesionSphericity + ΔGlobalEfficiency	AUC=0.800
mRS improved (12m)	Clinical	NIHSS_T0 + age + sex	AUC=0.969
FAC improved (12m)	Clinical + Disconnectome	NIHSS_T0 + ΔGlobalEfficiency + SMA_LI	AUC=0.952
FAC improved (12m)	Disconnectome	SMA_LateralityIndex + LesionVolume	AUC=0.829
FAC improved (12m)	Clinical	NIHSS_T0	AUC=0.794
Spasticity (12m)	Clinical + Disconnectome	NIHSS_T0 + WithinMotor_Delta_pct	AUC=0.771
Spasticity (12m)	Disconnectome	ΔGlobalEfficiency + SensoryIndex	AUC=0.625
Spasticity (12m)	Clinical	NIHSS_T0 + age + sex	AUC=0.859

Table 3. Predictive performance of clinical, disconnectome, and combined models across outcomes.

4.6 Inter-correlations between Clinical, Lesion, and Disconnectome Variables

To explore the underlying relationships between predictors and outcomes, a Spearman rank correlation analysis was performed across all numeric variables. The resulting correlation matrix revealed several distinct clusters of highly inter-correlated variables (Figure 17, Full Matrix). As expected, strong positive correlations were observed among baseline clinical severity metrics (Age, NIHSS T0 Total, NIHSS T0 Motor) and among various measures of lesion size and geometry (LesionVolume, LesionSurface, BoundingBoxVolume). Similarly, many of the disconnectome metrics formed their own correlated clusters; for instance, the nodal disconnection indices (M1, SMA, PMd) were strongly correlated with each other and with the composite MNDI and MNDI3 scores.

A more focused analysis on the relationships between core predictors and 12-month outcomes provided key insights into the structure of the data (Figure 18, Key Outcomes & Core Predictors). The three primary binary outcomes—poorer functional status (mRS ≥ 3), poorer ambulation (FAC≥ 3), and presence of spasticity—were all strongly and significantly inter-correlated, suggesting a shared underlying dimension of global post-stroke disability. These adverse outcomes were, in turn, most strongly correlated with higher baseline motor severity (NIHSS T0 Motor) and, to a lesser extent, with larger lesion volume.

Among the imaging metrics, ΔGlobal Efficiency and Lesion Sphericity showed the strongest and most consistent correlations with adverse long-term outcomes. Specifically, greater loss in global efficiency and more irregular lesion shapes were significantly associated with worse motor scores, poorer functional independence, and reduced ambulatory capacity at 12 months. In contrast, while nodal disconnection metrics like MNDI3 and M1/SMA laterality indices were powerful predictors in multivariate models, their direct bivariate correlations with outcomes were more moderate. This suggests that their predictive value is most potent when accounting for the shared variance with clinical and lesion-based measures, highlighting their role in capturing unique aspects of the underlying pathophysiology not fully represented by simpler metrics.

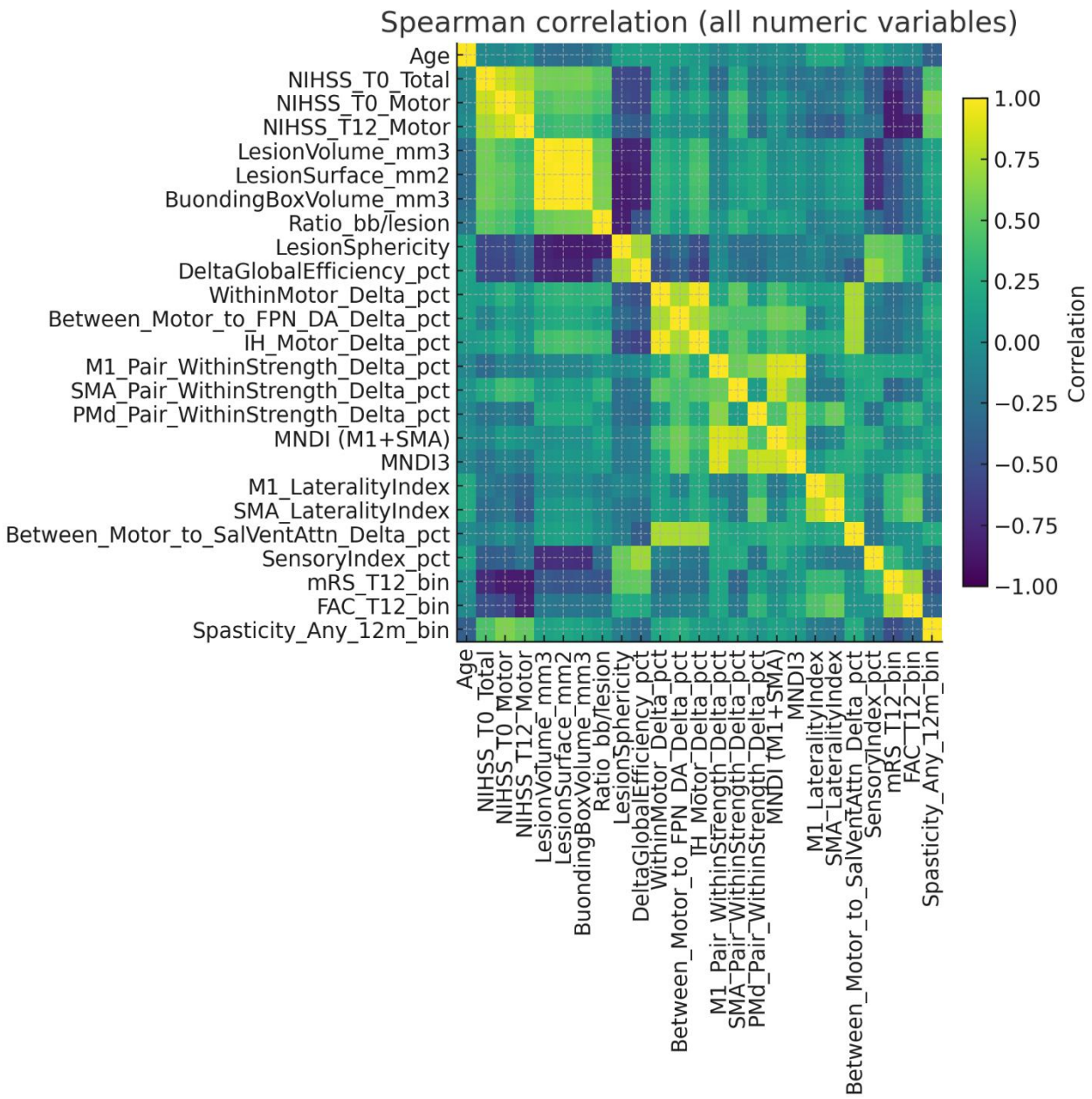

Figure 17 - Spearman correlation matrix of clinical, lesion, and disconnectome variables.

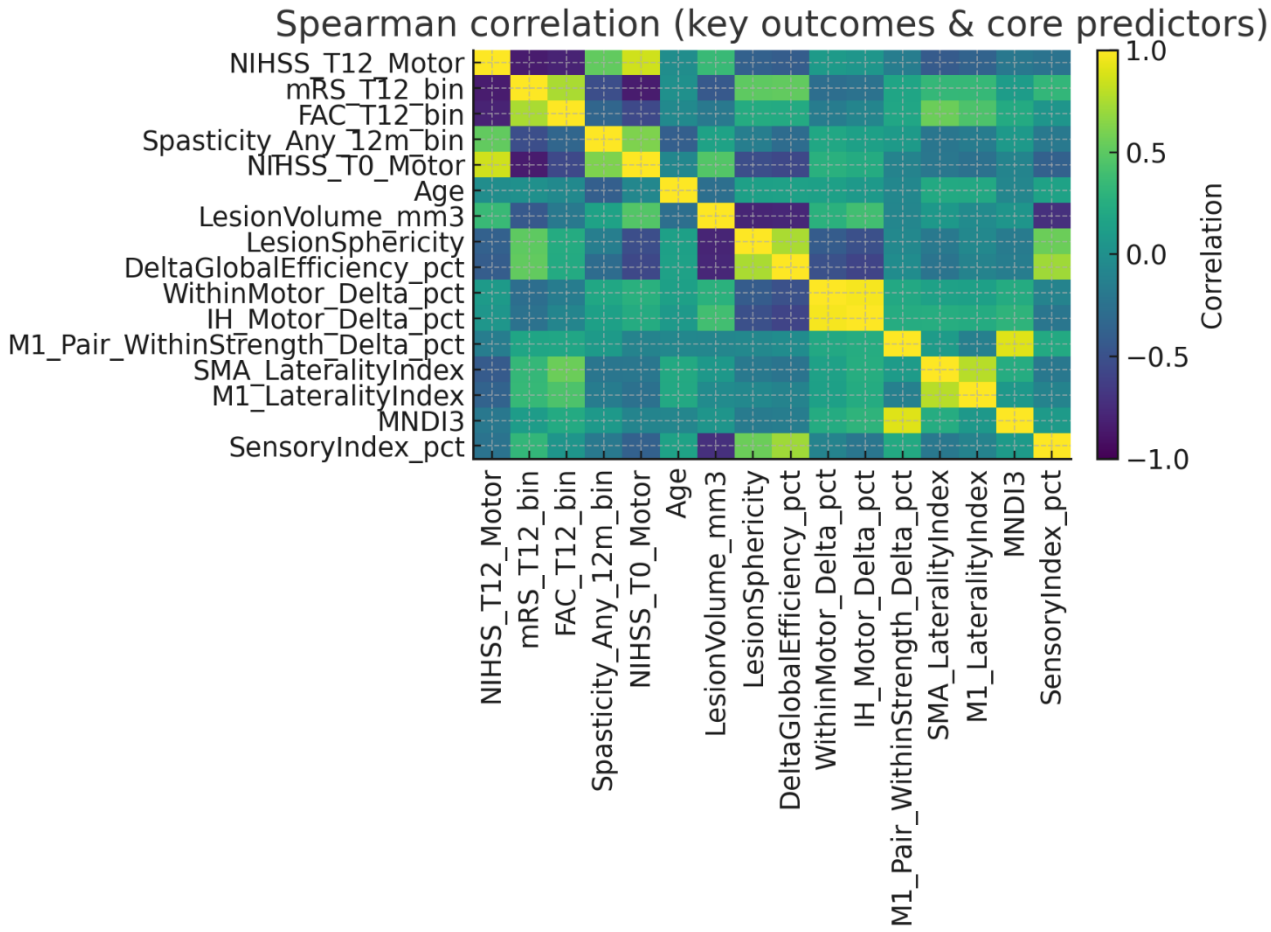

Figure 18 - Spearman correlation matrix of core predictors.

CHAPTER 5 - DISCUSSION

This thesis was designed to address a critical gap in stroke prognostication by investigating whether advanced metrics of brain network injury, derived from standard clinical scans, could enhance the prediction of long-term functional outcomes. The central aim was to move beyond traditional predictors like lesion volume and initial clinical severity, and to test the hypothesis that a more mechanistic measure—the structural disconnectome—provides superior and independent prognostic value. To achieve this, we quantified patient-specific lesion geometry and the resulting disruption to large-scale brain networks in a cohort of stroke survivors. We then developed and validated a series of multivariate models to predict three key, clinically relevant outcomes at 12 months: functional independence, ambulatory independence, and the development of spasticity.

5.1 Principal Findings

The central finding of this investigation is that a multi-modal prognostic approach, integrating baseline clinical data with advanced imaging metrics, could yield superior predictive accuracy for long-term stroke outcomes. While models based solely on imaging retained informative value, their performance was significantly enhanced by the inclusion of the initial clinical motor deficit. This underscores the synergistic, rather than redundant, nature of these two data streams. Crucially, this work demonstrates that metrics derived from the structural disconnectome provide significant and independent prognostic value, revealing distinct and biologically plausible predictive signatures for different facets of recovery.

A more nuanced interpretation of the results suggests that a single, universal biomarker is insufficient to capture the multifaceted nature of post-stroke recovery. For global functional independence (mRS ≤ 2), the analyses indicated that lesion geometry, particularly a deviation from a compact spherical shape, and composite motor network damage (MNDI3) were the most influential factors. In the final multivariate model, these mechanistic measures appeared to capture much of the predictive information contained within the initial clinical score. In contrast, ambulatory independence (FAC $\geq$ 4) seemed to be uniquely sensitive to metrics of network asymmetry, with the SMA Laterality Index

emerging as the most prominent predictor. This finding points towards the critical role of interhemispheric balance within higher-order motor planning networks for the recovery of complex functions like gait.

A distinct predictive pattern was observed for the development of spasticity. Here, the initial clinical severity of the motor deficit was the primary and most powerful predictor. While structural disconnection within the somatomotor network provided a statistically relevant but smaller contribution, the initial severity of the corticospinal insult appeared to be the dominant determinant. Taken together, these findings suggest a compelling dissociation: while a severe initial clinical deficit may be the principal driver of maladaptive plasticity leading to spasticity, the ultimate ceiling of functional and ambulatory recovery appears more closely tied to the specific topological and geometric characteristics of the brain injury and its consequent impact on large-scale network integrity.

5.2 Functional Independency

The prediction of global functional independence, as measured by the mRS at 12 months, was uniquely characterized by the combined influence of lesion geometry and network-level disconnection. This finding aligns with the established principle that lesion topography is often more critical than simple lesion volume for determining long-term outcome[68]. The emergence of Lesion Sphericity as the most powerful single predictor in both univariate and multivariate models is particularly insightful. A less spherical, more irregular lesion likely has a greater surface-area-to-volume ratio and is more liable to infiltrate and transect multiple, functionally distinct white matter fasciculi simultaneously. It can therefore be conceptualized as a powerful, albeit indirect, proxy for widespread, multi-domain network disruption, which logically translates to a greater global disability as captured by the mRS.

The independent predictive contribution of the Motor Network Disconnection Index further refines this picture. This result underscores the profound impact of motor impairment on overall disability, a feature that is heavily weighted in the hierarchical structure of the mRS[69] . The MNDI3 serves as a direct structural proxy for the integrity of the core corticospinal and cortico-subcortical motor systems. The preservation of these pathways, particularly the corticospinal tract, is a well-established prerequisite for substantial motor recovery, and its damage is a robust predictor of long-term motor deficits[70] .

5.3 Ambulatory Independency

The prediction of ambulatory independence presented a distinct neuroanatomical signature, dominated by metrics of interhemispheric balance and global network integrity rather than focal motor pathway damage. This finding suggests that the capacity for independent walking one year after stroke is contingent not just on the recovery of leg strength, but on the brain's preserved ability to orchestrate complex, bilateral motor programs.

The emergence of the SMA Laterality Index as the most powerful univariate and multivariate predictor is neurobiologically compelling. Bipedal locomotion is a highly complex task that requires the precise temporal coordination and integration of motor commands to both lower limbs heavily relying on interhemispheric cooperation[71]. The SMA is a critical hub for the planning, sequencing, and initiation of such internally generated, complex movements, and it plays a crucial role in interhemispheric coordination[72,73]. A high laterality index signifies a profound imbalance in the structural disconnection between the ipsilesional and contralesional SMA. This imbalance likely disrupts the fluid, rhythmic dialogue between the hemispheres that is essential for orchestrating the gait cycle, leading to deficits in balance, coordination, and timing that prevent independent ambulation.

The secondary, but significant, contribution of the loss in global network efficiency further supports this network-level interpretation. Walking is a resource-intensive process that demands the continuous integration of visual, proprioceptive, and vestibular information to maintain posture and adapt to the environment; is not merely a simple motor task but a resource-intensive process that demands significant cognitive resources, including attention and executive function, to integrate sensory information and maintain dynamic stability[74] . A reduction in global network efficiency reflects a diminished overall processing capacity of the surviving neural architecture, making it more difficult to perform such a complex, multi-domain task[75].

Notably, and in stark contrast to the findings for spasticity, the initial clinical motor severity was a minimal predictor of ambulatory outcome in the multivariate context. This dissociation suggests that while the NIHSS motor score effectively captures raw corticospinal output and limb strength, it fails to encapsulate the higher-order network dynamics essential for functional ambulation A patient may recover substantial leg strength but remain unable to walk independently due to a persistent network imbalance that impairs coordination and balance, a phenomenon consistent with the principle of maladaptive interhemispheric competition observed in motor recovery[76]. Therefore, our results posit that the capacity for independent walking at one year is less dependent on the initial degree of paresis and more contingent upon the brain's preserved ability to orchestrate complex motor plans through a balanced interhemispheric dialogue and an efficient global network.

5.4 Spasticity

The prediction of post-stroke spasticity revealed a distinct pattern that diverged significantly from the models for functional and ambulatory recovery. An initial analysis of lesion geometric properties revealed that patients who subsequently developed spasticity had, on average, substantially larger and more irregularly shaped lesions compared to those who did not (Median Lesion Volume: 28,890 mm^3 vs. 6,996 mm^3). However, consistent with the low univariate predictive power of these metrics (AUCs < 0.5), these differences in central tendency did not reach statistical significance in bivariate testing

(Mann-Whitney U, $p > 0.05$ for all lesion metrics). This lack of significance, despite the large difference in medians, is attributable to the high inter-patient variability in lesion characteristics within each outcome group and underscores that simple lesion metrics are insufficient standalone predictors of spasticity.

This finding shifts the focus towards more functional or network-based measures. Indeed, our multivariate models revealed that the overwhelmingly dominant predictor was the initial clinical severity of the motor deficit. This is biologically coherent, as spasticity is widely understood as an upper motor neuron syndrome resulting from the loss of descending inhibitory control over spinal reflex circuits. The NIHSS motor score is the most direct clinical measure of the functional integrity of the corticospinal tract in the acute phase[77]. A severe initial motor deficit is a direct manifestation of a profound disruption to these descending pathways, making it a logical and powerful predictor of a subsequent maladaptive consequence, like spasticity, that arises from that very same pathway disruption.

However, the finding that the degree of structural disconnection within the somatomotor network provided a smaller but independent contribution is equally important, as it refines our understanding of the underlying anatomy. While the NIHSS captures the functional output of the CST, this disconnectome metric quantifies the structural damage to the broader sensorimotor network, including cortico-subcortical loops. This aligns with a growing body of literature that implicates not only the direct pyramidal tracts but also key subcortical structures in the modulation of muscle tone. Voxel-based lesion-symptom mapping studies have consistently identified a network of regions—including the putamen, thalamus, internal capsule, insula, and corona radiata—as critical neuroanatomical correlates of spasticity [78,79]. Similarly, studies by Ri et al.[80,81] have consistently demonstrated that spasticity is more prevalent in patients with larger lesions involving not just the pyramidal tract but also the internal capsule, striatum, and thalamus. More recent work by Qin et al.[82], using a lesion network mapping approach, has further refined this by demonstrating that

heterogeneous lesions causing spasticity are functionally connected to a common network involving the bilateral putamen and globus pallidus. Our metric quantifying the disruption of connections internal to the somatomotor network is sensitive to the integrity of these cortico-striatal-thalamic circuits, which are crucial for modulating motor output. Therefore, while the initial NIHSS score reflects the severity of the primary corticospinal "hit," the additional measure of network disconnection likely captures the burden of damage to these critical modulatory circuits, explaining its role as a secondary, independent risk factor[83].

It is important to acknowledge that the current analysis is based on the disconnection of large-scale networks. A more granular investigation focusing on the disconnection of specific white matter tracts—such as the corticospinal, corticoreticular, and corticostriatal pathways—was beyond the scope of this initial work. Future studies from our group will explicitly perform tract-based disconnection analyses, which are expected to provide greater anatomical specificity and further validate the mechanistic link between the disruption of specific descending motor pathways and the development of spasticity. In conclusion, our current results suggest a model where the initial, severe clinical motor deficit acts as the primary trigger for spasticity, while the extent of structural disconnection within the broader sensorimotor network acts as a secondary modulator. This framework consistently demonstrates that while structural disconnection is a statistically relevant factor, the initial severity of the clinical motor insult remains the principal determinant of long-term post-stroke spasticity.

5.5 Motor Recovery

For the continuous outcome of 12-month motor status (NIHSS motor score), the predictive models underscored the combined importance of the initial clinical deficit and the structural extent of the brain injury. The optimal model, which integrated baseline motor severity, lesion volume, and the composite disconnectome score (MNDI3), explained a substantial portion of the variance in long-term motor outcomes ($R^2 = 0.66$). In stark contrast, an imaging-only model performed substantially

less well ($R^2 \approx 0.22$), highlighting that for predicting the final motor state, the starting point of the recovery trajectory—the initial severity of paresis—is an indispensable component. Within the full model, both larger lesion volume and greater nodal motor disconnection independently predicted a worse long-term motor deficit, even after accounting for baseline severity. This aligns with established principles of motor recovery, where the final outcome is constrained by both the initial functional impairment and the structural integrity of the underlying corticospinal system[84]. The finding that both lesion volume and disconnectome metrics contribute unique predictive information suggests that while lesion volume may capture the overall extent of tissue damage, the MNDI3 provides a more specific measure of the disruption to the critical, executive motor network, a factor known to be crucial for recovery[85]

5.6 Clinical Relevance

The findings of this thesis hold significant translational potential, suggesting a pathway to move beyond generalized prognostic statements and toward a more stratified and personalized approach to neurorehabilitation. The true value of an accurate prognostic model lies not in simply predicting a future state, but in its ability to inform present-day therapeutic strategy. This is particularly salient for the field of physiatry, where the primary goal is to optimize functional recovery by tailoring interventions to the individual patient's unique neurobiological substrate. Our results provide a framework for how disconnectome-based metrics, derivable from acute-phase imaging, could be integrated into this process, a concept supported by a growing body of research demonstrating that computational models based on the structural connectome can reliably predict individual recovery trajectories[51,86].

A primary implication is the potential for early patient stratification to guide rehabilitative strategies. For instance, our models for functional and ambulatory independence were powerfully driven by metrics of lesion geometry and network asymmetry. A patient presenting with a highly non-spherical, spatially dispersed lesion or a severe imbalance in the disconnection of the supplementary motor area

(SMA) could be identified at admission as having a high probability of a more challenging and incomplete recovery. For such a patient, a physiatrist could make an early, evidence-based decision to shift the therapeutic focus from purely restorative goals towards compensatory strategies. This might involve the early introduction of assistive technologies, environmental modifications, and task-specific training that prioritizes functional independence within the predicted limits of recovery, thereby managing patient and family expectations and optimizing the allocation of rehabilitative resources. While recent large-scale studies, such as that by Sperber et al. [87], have argued that simple spatial lesion features may be sufficient for predicting global outcomes, our findings suggest a more nuanced picture. For highly specific, functionally critical outcomes like independent ambulation, network-specific metrics such as the SMA Laterality Index provide superior and unique predictive information that is not captured by lesion geometry alone, aligning with research that shows connectomic markers are particularly valuable for modeling specific post-stroke cognitive and motor deficits.

Furthermore, our findings provide a clear rationale for a proactive approach to spasticity management. The dominant predictive role of the initial NIHSS motor score allows for the immediate identification of a high-risk population. These patients could be enrolled in proactive "spasticity surveillance" protocols, with more frequent monitoring and the preemptive application of interventions aimed at mitigating this debilitating secondary impairment. This is particularly relevant given the consistent implication of a network of subcortical structures—including the putamen, thalamus, internal capsule, and corona radiata—in the development of spasticity[78,79] . The secondary predictive role of disconnection within the motor network in our models likely reflects the structural substrate of this well-documented anatomical vulnerability.

Finally, looking forward, the disconnectome map itself could evolve from a prognostic tool into a therapeutic guide for innovative interventions. As our understanding of network dynamics improves, the patient-specific map of structural disconnection could serve as a target for neuromodulatory

techniques like repetitive Transcranial Magnetic Stimulation (rTMS) or transcranial Direct Current Stimulation (tDCS). A patient with a profound SMA imbalance, for example, might be an ideal candidate for targeted rTMS protocols designed to rebalance interhemispheric inhibition. This vision aligns with the broader goal of integrating advanced imaging into clinical workflows to create "personalized therapy regimens"[88]. The feasibility of deriving such complex network information from routinely collected clinical MR images, as demonstrated in studies on language recovery[89] , constitutes a "significant advancement toward practical clinical application" and paves the way for a future where a patient's unique "disconnectome fingerprint" is used not only to predict their recovery but also to guide the selection of mechanistically-driven therapies.

5.7 Limitations

While this study provides novel insights into the prognostic value of network-based biomarkers, its findings must be interpreted in the context of several important limitations.

First, the sample size, while sufficient for the development of robust internal models, is relatively modest. This constrains the statistical power for subgroup analyses and limits the generalizability of our findings to the broader, highly heterogeneous stroke population. The inclusion of both ischemic and hemorrhagic strokes, while reflecting clinical reality, introduces additional variance that may obscure more subtle relationships.

Second, our methodology relies on an indirect, atlas-based approach to quantify structural disconnection. This technique operates on the fundamental assumption that the patient's pre-morbid neuroanatomy conforms to the healthy, normative connectome atlas used as a reference. This does not account for individual neuroanatomical variability and, critically, introduces a potential confound due to the age mismatch between the typically young adult cohorts used to build reference atlases and our significantly older stroke patient population, which may have pre-existing age-related white matter changes.

Third, the scope of our investigation, while broad, included only a subset of all existing connectomic measures. Our focus was on structural disconnection, but other representations of a stroke lesion exist, including direct or indirect measures of functional connectivity. Directly acquired connectomic data, both structural (via patient-specific DTI) and functional (via rs-fMRI), might provide better predictors, but this would come at the price of dedicated and complex imaging sequences and post-processing, thereby reducing the immediate clinical applicability that was a core goal of this study.

Fourth, the processing of high-dimensional imaging data introduces an enormous number of methodological degrees of freedom. The choices made in the current study—including the focus on structural connectivity, the selection of a specific connectome reference atlas, the use of a particular processing toolbox, and the utilization of a single prediction algorithm—all influence the final results. Future work, especially with larger consortia datasets, could explore the tuning of various hyperparameters and the application of more complex machine learning or deep learning algorithms, which may further improve predictive accuracy.

Finally, the informative value of any imaging marker is inherently limited because other clinical and demographic variables play a crucial role in recovery. Factors such as brain reserve, underlying comorbidities, and, critically, the type and dose of rehabilitation received are powerful modulators of outcome. The observational nature of this study precluded the standardization of rehabilitative interventions, which remains a significant unmeasured confounder.

5.8 Conclusions

This dissertation has demonstrated that metrics of structural disconnection, derived from acute-phase clinical imaging, provide robust and independent prognostic value for long-term outcomes following stroke. By moving beyond traditional predictors, this work establishes that the anatomical "fingerprint" of a lesion—encompassing its geometry, its impact on global network efficiency, and its disruption of specific network nodes and pathways—is a critical determinant of a patient's recovery

trajectory. Crucially, this research moves beyond the search for a single, universal biomarker, revealing instead that distinct facets of recovery are governed by distinct and biologically plausible predictive signatures. We found that global functional independence is most strongly predicted by a combination of lesion geometry and composite motor network damage; ambulatory independence is uniquely sensitive to the interhemispheric balance of the supplementary motor area; and the development of spasticity is overwhelmingly driven by the initial severity of the clinical motor deficit. This dissociation underscores that a "one-size-fits-all" prognostic approach is insufficient for capturing the complex and multifaceted nature of post-stroke recovery.

The findings presented herein represent a foundational step toward the clinical implementation of a stratified and personalized approach to neurorehabilitation. By providing a framework to identify patient-specific patterns of network vulnerability in the acute phase, this work offers a potential pathway to guide more targeted therapeutic strategies, set more realistic rehabilitative goals, and proactively manage secondary complications. Ultimately, this research provides a robust proof-of-concept for translating complex neuroimaging data into clinically actionable insights, paving the way for a future of precision neurorehabilitation where therapeutic interventions are tailored to the unique network-level pathology of the individual patient.

REFERENCES

1. Feigin VL, Stark BA, Johnson CO, et al. Global, regional, and national burden of stroke and its risk factors, 1990-2019: A systematic analysis for the Global Burden of Disease Study 2019. *Lancet Neurol*. 2021;20:1–26.

2. Hankey GJ. Stroke. *The Lancet*. 2017;389:641–654.

3. Adams HP, Davis PH, Leira EC, et al. Baseline NIH Stroke Scale score strongly predicts outcome after stroke: A report of the Trial of Org 10172 in Acute Stroke Treatment (TOAST). *Neurology*. 1999;53:126–131. Available at: https://pubmed.ncbi.nlm.nih.gov/10408548/. Accessed September 17, 2025.

4. Leira EC, Coffey CS, Jorge RE, et al. The NIHSS supplementary motor scale: A valid tool for multidisciplinary recovery trials. *Cerebrovascular Diseases*. 2013;36:69–73.

5. Gladstone DJ, Danells CJ, Black SE. The fugl-meyer assessment of motor recovery after stroke: a critical review of its measurement properties. *Neurorehabil Neural Repair*. 2002;16:232–240. Available at: https://pubmed.ncbi.nlm.nih.gov/12234086/. Accessed September 17, 2025.

6. Sperber C, Gallucci L, Mirman D, Arnold M, Umarova RM. Stroke lesion size – Still a useful biomarker for stroke severity and outcome in times of high-dimensional models. *Neuroimage Clin*. 2023;40.

7. Vogt G, Laage R, Shuaib A, Schneider A. Initial lesion volume is an independent predictor of clinical stroke outcome at day 90: An analysis of the Virtual International Stroke Trials Archive (VISTA) database. *Stroke*. 2012;43:1266–1272.

8. Bang OY, Park HY, Yoon JH, et al. Predicting the Long-Term Outcome after Subacute Stroke within the Middle Cerebral Artery Territory. *J Clin Neurol*. 2005;1:148. Available at: https://pmc.ncbi.nlm.nih.gov/articles/PMC2854920/. Accessed September 17, 2025.

9. Grefkes C, Grefkes C, Fink GR, Fink GR. Recovery from stroke: Current concepts and future perspectives. *Neurol Res Pract*. 2020;2:1–10. Available at: https://neurolrespract.biomedcentral.com/articles/10.1186/s42466-020-00060-6. Accessed September 17, 2025.

10. Sporns O, Tononi G, Kötter R. The human connectome: A structural description of the human brain. *PLoS Comput Biol*. 2005;1:0245–0251. Available at: https://pubmed.ncbi.nlm.nih.gov/16201007/. Accessed September 17, 2025.

11. Silasi G, Murphy TH. Stroke and the connectome: How connectivity guides therapeutic intervention. *Neuron*. 2014;83:1354–1368.

12. Stinear CM, Lang CE, Zeiler S, Byblow WD. Advances and challenges in stroke rehabilitation. *Lancet Neurol*. 2020;19:348–360. Available at: https://pubmed.ncbi.nlm.nih.gov/32004440/. Accessed September 17, 2025.

13. Ahmed N, Audebert H, Turc G, et al. Consensus statements and recommendations from the ESO-Karolinska Stroke Update Conference, Stockholm 11–13 November 2018. *Eur Stroke J*. 2019;4:307–317.

14. Quinn TJ, Richard E, Teuschl Y, et al. European Stroke Organisation and European Academy of Neurology joint guidelines on post-stroke cognitive impairment. *Eur Stroke J*. 2021;6:I–XXXVIII.

15. Morone G, Pichiorri F. Post-Stroke Rehabilitation: Challenges and New Perspectives. *J Clin Med*. 2023;12:550. Available at: https://pmc.ncbi.nlm.nih.gov/articles/PMC9867345/. Accessed September 17, 2025.

16. Feigin VL, Abate MD, Abate YH, et al. Global, regional, and national burden of stroke and its risk factors, 1990–2021: a systematic analysis for the Global Burden of Disease Study 2021. *Lancet Neurol*. 2024;23:973–1003.

17. Feigin VL, Owolabi MO, Feigin VL, et al. Pragmatic solutions to reduce the global burden of stroke: a World Stroke Organization–Lancet Neurology Commission. *Lancet Neurol*. 2023;22:1160–1206.

18. Feigin VL, Brainin M, Norrving B, et al. World Stroke Organization: Global Stroke Fact Sheet 2025. *International Journal of Stroke*. 2025;20:132. Available at: https://pmc.ncbi.nlm.nih.gov/articles/PMC11786524/. Accessed September 13, 2025.

19. Boehme AK, Esenwa C, Elkind MSV. Stroke Risk Factors, Genetics, and Prevention. *Circ Res*. 2017;120:472. Available at: https://pmc.ncbi.nlm.nih.gov/articles/PMC5321635/. Accessed September 13, 2025.

20. Li L, Scott CA, Rothwell PM. Association of Younger vs Older Ages With Changes in Incidence of Stroke and Other Vascular Events, 2002-2018. *JAMA*. 2022;328:563–574. Available at: https://jamanetwork.com/journals/jama/fullarticle/2795026. Accessed September 17, 2025.

21. Coupland AP, Thapar A, Qureshi MI, Jenkins H, Davies AH. The definition of stroke. *J R Soc Med*. 2017;110:9. Available at: https://pmc.ncbi.nlm.nih.gov/articles/PMC5298424/. Accessed September 13, 2025.

22. Sacco RL, Kasner SE, Broderick JP, et al. An Updated Definition of Stroke for the 21st Century. *Stroke*. 2013;44:2064–2089. Available at: /doi/pdf/10.1161/STR.0b013e318296aeca?download=true. Accessed September 13, 2025.

23. Adams HP, Bendixen BH, Kappelle ; L Jaap, et al. Classification of subtype of acute ischemic stroke. Definitions for use in a multicenter clinical trial. TOAST. Trial of Org 10172 in Acute Stroke Treatment. *Stroke*. 1993;24:35–41. Available at: https://www.ahajournals.org/doi/abs/10.1161/01.str.24.1.35. Accessed November 18, 2021.

24. Kolominsky-Rabas PL, Weber M, Gefeller O, Neundoerfer B, Heuschmann PU. Epidemiology of ischemic stroke subtypes according to TOAST criteria: Incidence, recurrence, and long-term survival in ischemic stroke subtypes: A population-based study. *Stroke*. 2001;32:2735–2740.

25. Adams HP, Biller J. Classification of Subtypes of Ischemic Stroke. *Stroke*. 2015;46:e114–e117.

26. Puy L, Parry-Jones AR, Sandset EC, Dowlatshahi D, Ziai W, Cordonnier C. Intracerebral haemorrhage. *Nat Rev Dis Primers*. 2023;9.

27. Bernhardt J, Hayward KS, Kwakkel G, et al. Agreed definitions and a shared vision for new standards in stroke recovery research: The Stroke Recovery and Rehabilitation Roundtable taskforce. *International Journal of Stroke*. 2017;12:444–450. Available at: https://journals.sagepub.com/doi/10.1177/1747493017711816?url_ver=Z39.88-2003&rfr_id=ori%3Arid%3Acrossref.org&rfr_dat=cr_pub++0pubmed. Accessed September 13, 2025.

28. Langhorne P, Bernhardt J, Kwakkel G. Stroke rehabilitation. *The Lancet*. 2011;377:1693–1702. Available at: http://www.thelancet.com/article/S0140673611603255/fulltext. Accessed November 18, 2021.

29. Langhorne P, Coupar F, Pollock A. Motor recovery after stroke: a systematic review. *Lancet Neurol*. 2009;8:741–754.

30. Hope TMH, Friston K, Price CJ, Leff AP, Rotshtein P, Bowman H. Recovery after stroke: Not so proportional after all? *Brain*. 2019;142.

31. Winstein CJ, Stein J, Arena R, et al. Guidelines for Adult Stroke Rehabilitation and Recovery: A Guideline for Healthcare Professionals from the American Heart Association/American Stroke Association. *Stroke*. 2016;47.

32. Kane E, Ward NS. Neurobiology of Stroke Recovery. *Clinical Pathways in Stroke Rehabilitation: Evidence-based Clinical Practice Recommendations*. 2021:1–13. Available at: https://pubmed.ncbi.nlm.nih.gov/36315699/. Accessed September 17, 2025.

33. Seitz RJ, Azari NP, Knorr U, Binkofski F, Herzog H, Freund HJ. The role of diaschisis in stroke recovery. *Stroke*. 1999;30:1844–1850. Available at: https://pubmed.ncbi.nlm.nih.gov/10471434/. Accessed September 17, 2025.

34. Toga AW, Clark KA, Thompson PM, Shattuck DW, Van Horn JD. Mapping the Human Connectome. *Neurosurgery*. 2012;71:1. Available at: https://pmc.ncbi.nlm.nih.gov/articles/PMC3555558/. Accessed September 17, 2025.

35. Grier MD, Zimmermann J, Heilbronner SR. Estimating brain connectivity with diffusion-weighted MRI: Promise and peril. *Biol Psychiatry Cogn Neurosci Neuroimaging*. 2020;5:846. Available at: https://pmc.ncbi.nlm.nih.gov/articles/PMC7483308/. Accessed September 17, 2025.

36. Mori S, Barker PB. Diffusion Magnetic Resonance Imaging: Its Principle and Applications. *Anat Rec (New Anat)*. 1999;257:102–109. Available at: /doi/pdf/10.1002/%28SICI%291097-0185%2819990615%29257%3A3%3C102%3A%3AAID-AR7%3E3.0.CO%3B2-6. Accessed September 17, 2025.

37. Luypaert R, Boujraf S, Sourbron S, Osteaux M. Diffusion and perfusion MRI: Basic physics. *Eur J Radiol*. 2001;38:19–27.

38. Alexander AL, Lee JE, Lazar M, Field AS. Diffusion Tensor Imaging of the Brain. *Neurotherapeutics*. 2007;4:316–329. Available at: https://www.sciencedirect.com/science/article/pii/S1878747923006530. Accessed September 17, 2025.

39. Le Bihan D, Mangin JF, Poupon C, et al. Diffusion tensor imaging: Concepts and applications. *Journal of Magnetic Resonance Imaging*. 2001;13:534–546.

40. Assaf Y, Pasternak O. Diffusion tensor imaging (DTI)-based white matter mapping in brain research: A review. *Journal of Molecular Neuroscience*. 2008;34:51–61.

41. Horsfield MA, Jones DK. Applications of diffusion-weighted and diffusion tensor MRI to white matter diseases - A review. *NMR Biomed*. 2002;15:570–577.

42. Pierpaoli C, Jezzard P, Basser PJ, Barnett A, Di Chiro G. Diffusion tensor MR imaging of the human brain. *Radiology*. 1996;201:637–648.

43. Le Bihan D, Breton E, Lallemand D, Grenier P, Cabanis E, Laval-Jeantet M. MR imaging of intravoxel incoherent motions: Application to diffusion and perfusion in neurologic disorders. *Radiology*. 1986;161:401–407.

44. Lv H, Wang Z, Tong E, et al. Resting-State Functional MRI: Everything That Nonexperts Have Always Wanted to Know. *AJNR Am J Neuroradiol*. 2018;39:1390. Available at: https://pmc.ncbi.nlm.nih.gov/articles/PMC6051935/. Accessed September 17, 2025.

45. Ogawa S, Lee TM, Kay AR, Tank DW. Brain magnetic resonance imaging with contrast dependent on blood oxygenation. *Proc Natl Acad Sci U S A*. 1990;87:9868–9872.

46. Nasrallah FA, Yeow LY, Biswal B, Chuang KH. Dependence of BOLD signal fluctuation on arterial blood CO2 and O2: Implication for resting-state functional connectivity. *Neuroimage*. 2015;117:29–39.

47. Wegener S. Neuroimaging of Acute Ischaemic Stroke: Current Challenges. *EMJ Neurol Neurology 1.1 2014*. 2014;1:49–52. Available at: https://www.emjreviews.com/neurology/article/neuroimaging-of-acute-ischaemic-stroke-current-challenges/. Accessed September 17, 2025.

48. Behrens TEJ, Sporns O. Human connectomics. *Curr Opin Neurobiol*. 2012;22:144–153.

49. Van Essen DC, Ugurbil K, Auerbach E, et al. The Human Connectome Project: A data acquisition perspective. *Neuroimage*. 2012;62:2222. Available at: https://pmc.ncbi.nlm.nih.gov/articles/PMC3606888/. Accessed September 17, 2025.

50. Glasser MF, Smith SM, Marcus DS, et al. The Human Connectome Project's neuroimaging approach. *Nat Neurosci*. 2016;19:1175–1187. Available at: https://www.nature.com/articles/nn.4361. Accessed September 17, 2025.

51. Rivier C, Preti MG, Nicolo P, Van De Ville D, Guggisberg AG, Pirondini E. Prediction of post-stroke motor recovery benefits from measures of sub-acute widespread network damages. *Brain Commun*. 2023;5. Available at: https://dx.doi.org/10.1093/braincomms/fcad055. Accessed September 16, 2025.

52. Saver JL, Chaisinanunkul N, Campbell BCV, et al. Standardized Nomenclature for Modified Rankin Scale Global Disability Outcomes: Consensus Recommendations from Stroke Therapy Academic Industry Roundtable XI. *Stroke*. 2021:3054–3062. Available at: https://www.ahajournals.org/doi/abs/10.1161/STROKEAHA.121.034480. Accessed November 18, 2021.

53. Quinn TJ, Dawson J, Walters MR, Lees KR. Exploring the reliability of the modified rankin scale. *Stroke*. 2009;40:762–766. Available at: https://pubmed.ncbi.nlm.nih.gov/19131664/. Accessed February 27, 2022.

54. Collen FM, Wade DT, Bradshaw CM. Mobility after stroke: reliability of measures of impairment and disability. *Int Disabil Stud*. 1990;12:6–9. Available at: https://pubmed.ncbi.nlm.nih.gov/2211468/. Accessed September 17, 2025.

55. Holden MK, Gill KM, Magliozzi MR. Gait assessment for neurologically impaired patients. Standards for outcome assessment. *Phys Ther*. 1986;66:1530–1539. Available at: https://pubmed.ncbi.nlm.nih.gov/3763704/. Accessed September 17, 2025.

56. Pandyan AD, Johnson GR, Price CIM, Curless RH, Barnes MP, Rodgers H. A review of the properties and limitations of the Ashworth and modified Ashworth Scales as measures of spasticity: *http://dx.doi.org/10.1191/026921599677595404*. 2016;13:373–383. Available at: https://journals.sagepub.com/doi/abs/10.1191/026921599677595404?journalCode=crea. Accessed September 16, 2021.

57. Brett M, Johnsrude IS, Owen AM. The problem of functional localization in the human brain. *Nat Rev Neurosci*. 2002;3:243–249. Available at: https://www.nature.com/articles/nrn756. Accessed September 17, 2025.

58. Cheng B, Knaack C, Forkert ND, Schnabel R, Gerloff C, Thomalla G. Stroke subtype classification by geometrical descriptors of lesion shape. *PLoS One*. 2017;12:e0185063. Available at: https://pmc.ncbi.nlm.nih.gov/articles/PMC5720627/. Accessed September 3, 2025.

59. Kuceyeski A, Maruta J, Relkin N, Raj A. The Network Modification (NeMo) Tool: Elucidating the Effect of White Matter Integrity Changes on Cortical and Subcortical Structural Connectivity. *Brain Connect*. 2013;3:451. Available at: https://pmc.ncbi.nlm.nih.gov/articles/PMC3796322/. Accessed September 17, 2025.

60. Kuceyeski A, Maruta J, Relkin N, Raj A. The Network Modification (NeMo) Tool: Elucidating the Effect of White Matter Integrity Changes on Cortical and Subcortical Structural Connectivity.

https://home.liebertpub.com/brain. 2013;3:451–463. Available at: /doi/pdf/10.1089/brain.2013.0147?download=true. Accessed September 17, 2025.

61. Thomas Yeo BT, Krienen FM, Sepulcre J, et al. The organization of the human cerebral cortex estimated by intrinsic functional connectivity. *J Neurophysiol*. 2011;106:1125–1165. Available at: https://pubmed.ncbi.nlm.nih.gov/21653723/. Accessed September 17, 2025.

62. Schaefer A, Kong R, Gordon EM, et al. Local-Global Parcellation of the Human Cerebral Cortex from Intrinsic Functional Connectivity MRI. *Cereb Cortex*. 2018;28:3095–3114. Available at: https://pubmed.ncbi.nlm.nih.gov/28981612/. Accessed September 17, 2025.

63. Pedregosa FABIANPEDREGOSA F, Michel V, Grisel OLIVIERGRISEL O, et al. Scikit-learn: Machine Learning in Python Gaël Varoquaux Bertrand Thirion Vincent Dubourg Alexandre Passos PEDREGOSA, VAROQUAUX, GRAMFORT ET AL. Matthieu Perrot. *Journal of Machine Learning Research*. 2011;12:2825–2830. Available at: http://scikit-learn.sourceforge.net. Accessed September 14, 2025.

64. Karl L w. Description of the research used to generate our Data. *Description of the research used to generate our Data*. 2014:175–184. Available at: https://books.google.com/books/about/Regression_Modeling_Strategies.html?hl=it&id=sQ90rgEACAAJ. Accessed September 14, 2025.

65. Ziegler A. Clinical prediction models: A practical approach to development, validation, and updating Ewout W. Steyerberg (2019). Second Edition, Springer Series Statistics for Biology and Health. Cham: Springer. 558 pages. ISBN: 978-3-030-16398-3. https://doi.org/10.1007/978-3-030-16399-0. *Biometrical Journal*. 2020;62:1122–1123. Available at: /doi/pdf/10.1002/bimj.202000088. Accessed September 14, 2025.

66. Harrell , FE. Regression Modeling Strategies With Applications to Linear Models, Logistic and Ordinal Regression, and Survival Analysis. 2015. Available at: https://www.academia.edu/43291466/Regression_Modeling_Strategies_With_Applications_to_Linear_Models_Logistic_and_Ordinal_Regression_and_Survival_Analysis. Accessed September 14, 2025.

67. Moons KGM, Altman DG, Reitsma JB, et al. Transparent Reporting of a multivariable prediction model for Individual Prognosis or Diagnosis (TRIPOD): explanation and elaboration. *Ann Intern Med*. 2015;162:W1–W73. Available at: https://pubmed.ncbi.nlm.nih.gov/25560730/. Accessed September 14, 2025.

68. Wu O, Cloonan L, Mocking SJT, et al. Role of Acute Lesion Topography in Initial Ischemic Stroke Severity and Long-Term Functional Outcomes. *Stroke*. 2015;46:2438–2444. Available at: https://pubmed.ncbi.nlm.nih.gov/26199314/. Accessed September 16, 2025.

69. Banks JL, Marotta CA. Outcomes validity and reliability of the modified Rankin scale: implications for stroke clinical trials: a literature review and synthesis. *Stroke*. 2007;38:1091–1096. Available at: https://pubmed.ncbi.nlm.nih.gov/17272767/. Accessed September 16, 2025.

70. Stinear CM, Barber PA, Petoe M, Anwar S, Byblow WD. The PREP algorithm predicts potential for upper limb recovery after stroke. *Brain*. 2012;135:2527–2535. Available at: https://pubmed.ncbi.nlm.nih.gov/22689909/. Accessed September 16, 2025.

71. Grefkes C, Fink GR. Connectivity-based approaches in stroke and recovery of function. *Lancet Neurol*. 2014;13:206–216. Available at: https://www.thelancet.com/action/showFullText?pii=S1474442213702643. Accessed September 16, 2025.

72. Nachev P, Kennard C, Husain M. Functional role of the supplementary and pre-supplementary motor areas. *Nat Rev Neurosci*. 2008;9:856–869. Available at: https://pubmed.ncbi.nlm.nih.gov/18843271/. Accessed September 16, 2025.

73. Takakusaki K. Functional Neuroanatomy for Posture and Gait Control. *J Mov Disord*. 2017;10:1. Available at: https://pmc.ncbi.nlm.nih.gov/articles/PMC5288669/. Accessed September 16, 2025.

74. Yogev-Seligmann G, Hausdorff JM, Giladi N. The role of executive function and attention in gait. *Movement Disorders*. 2008;23:329–342. Available at: /doi/pdf/10.1002/mds.21720. Accessed September 16, 2025.

75. Wang L, Yu C, Chen H, et al. Dynamic functional reorganization of the motor execution network after stroke. *Brain*. 2010;133:1224–1238. Available at: https://dx.doi.org/10.1093/brain/awq043. Accessed September 16, 2025.

76. Murase N, Duque J, Mazzocchio R, Cohen LG. Influence of interhemispheric interactions on motor function in chronic stroke. *Ann Neurol*. 2004;55:400–409. Available at: /doi/pdf/10.1002/ana.10848. Accessed September 16, 2025.

77. Lindenberg R, Renga V, Zhu LL, Betzler F, Alsop D, Schlaug G. Structural integrity of corticospinal motor fibers predicts motor impairment in chronic stroke. *Neurology*. 2010;74:280–287.

78. Cheung DK, Climans SA, Black SE, Gao F, Szilagyi GM, Mochizuki G. Lesion Characteristics of Individuals with Upper Limb Spasticity after Stroke. *Neurorehabil Neural Repair*. 2016;30:63–70.

79. Lee KB, Hong BY, Kim JS, et al. Which brain lesions produce spasticity? An observational study on 45 stroke patients. *PLoS One*. 2019;14.

80. Ri S, Kivi A, Urban PP, Wolf T, Wissel J. Site and size of lesion predict post-stroke spasticity: A retrospective magnetic resonance imaging study. *J Rehabil Med*. 2020;52. Available at: https://pubmed.ncbi.nlm.nih.gov/32179931/. Accessed September 15, 2025.

81. Songjin RI, Glaess-Leistner S, Wissel J. Early brain imaging predictors of post-stroke spasticity. *J Rehabil Med*. 2021;53.

82. Qin Y, Qiu S, Liu X, et al. Lesions causing post-stroke spasticity localize to a common brain network. *Front Aging Neurosci*. 2022;14.

83. Cho MJ, Yeo SS, Lee SJ, Jang SH. Correlation between spasticity and corticospinal/corticoreticular tract status in stroke patients after early stage. *Medicine (United States)*. 2023;102:E33604.

84. Stinear CM. Prediction of motor recovery after stroke: advances in biomarkers. *Lancet Neurol*. 2017;16:826–836.

85. Boyd LA, Hayward KS, Ward NS, et al. Biomarkers of stroke recovery: Consensus-based core recommendations from the Stroke Recovery and Rehabilitation Roundtable. *Int J Stroke*. 2017;12:480–493. Available at: https://pubmed.ncbi.nlm.nih.gov/28697711/. Accessed September 16, 2025.

86. Koch PJ, Park CH, Girard G, et al. The structural connectome and motor recovery after stroke: Predicting natural recovery. *Brain*. 2021;144:2107–2119.

87. Sperber C, Gallucci L, Kasties V, Arnold M, Umarova RM. Connectomic stroke lesion measures provide no benefit over basic spatial lesion features in the prognosis of global stroke outcome measures. *Brain Commun*. 2025;7. Available at: https://pubmed.ncbi.nlm.nih.gov/40726767/. Accessed August 29, 2025.

88. Bonkhoff AK, Rehme AK, Hensel L, et al. Dynamic connectivity predicts acute motor impairment and recovery post-stroke. *Brain Commun*. 2021;3.

89. Hildesheim FE, Ophey A, Zumbansen A, et al. Predicting Language Function Post-Stroke: A Model-Based Structural Connectivity Approach. *Neurorehabil Neural Repair*. 2024;38:447–459.

APPENDIX

A. Representative Case Studies of Lesion and Disconnectome Mapping

The following pages provide a visual summary of the analytical pipeline for four representative patients from the study cohort. Each case illustrates the progression from the segmented anatomical lesion mask to the derived maps of structural disconnection, including the Change in Connectivity (ChaCo) scores, the projection of disconnection onto the Yeo-7 resting-state networks, and the final structural disconnectome map. These examples were chosen to demonstrate the application of the methodology across different lesion locations and sizes.

- *(Top Row) Lesion Mask*: The patient's specific lesion, located in the left fronto-parietal region, is shown as a binary mask (purple) after manual segmentation and normalization into MNI standard space. The color bar indicates the probability of a voxel being part of the lesion (1 = within the lesion).
- *(Second Row) ChaCo Score Map*: The Change in Connectivity (ChaCo) score is displayed, reflecting the severity of structural disconnection at a voxel-wise level. Higher scores (brighter yellow/white) indicate voxels whose structural connectivity profile has been most severely altered by the lesion. The map highlights a widespread impact extending far beyond the anatomical boundaries of the lesion itself, particularly affecting ipsilesional white matter tracts.
- *(Third Row) Yeo-7 Network Disconnection*: The structural disconnection is projected onto the seven canonical resting-state networks as defined by the Yeo et al. atlas. The color intensity represents the percentage of disconnection within each network parcel, revealing a non-uniform pattern of network vulnerability. The black overlay indicates regions with the most severe disconnection.

- *(Bottom Row) Structural Disconnectome:* A glass brain visualization of the inferred structural disconnectome. The black lines represent the specific white matter streamlines from a normative connectome atlas that were intersected by the patient's lesion mask. The colored dots represent the cortical endpoints of these disconnected streamlines, color-coded by their respective Yeo-7 network affiliation.

PATIENT 1 – Hischemic lesion right hemisphere

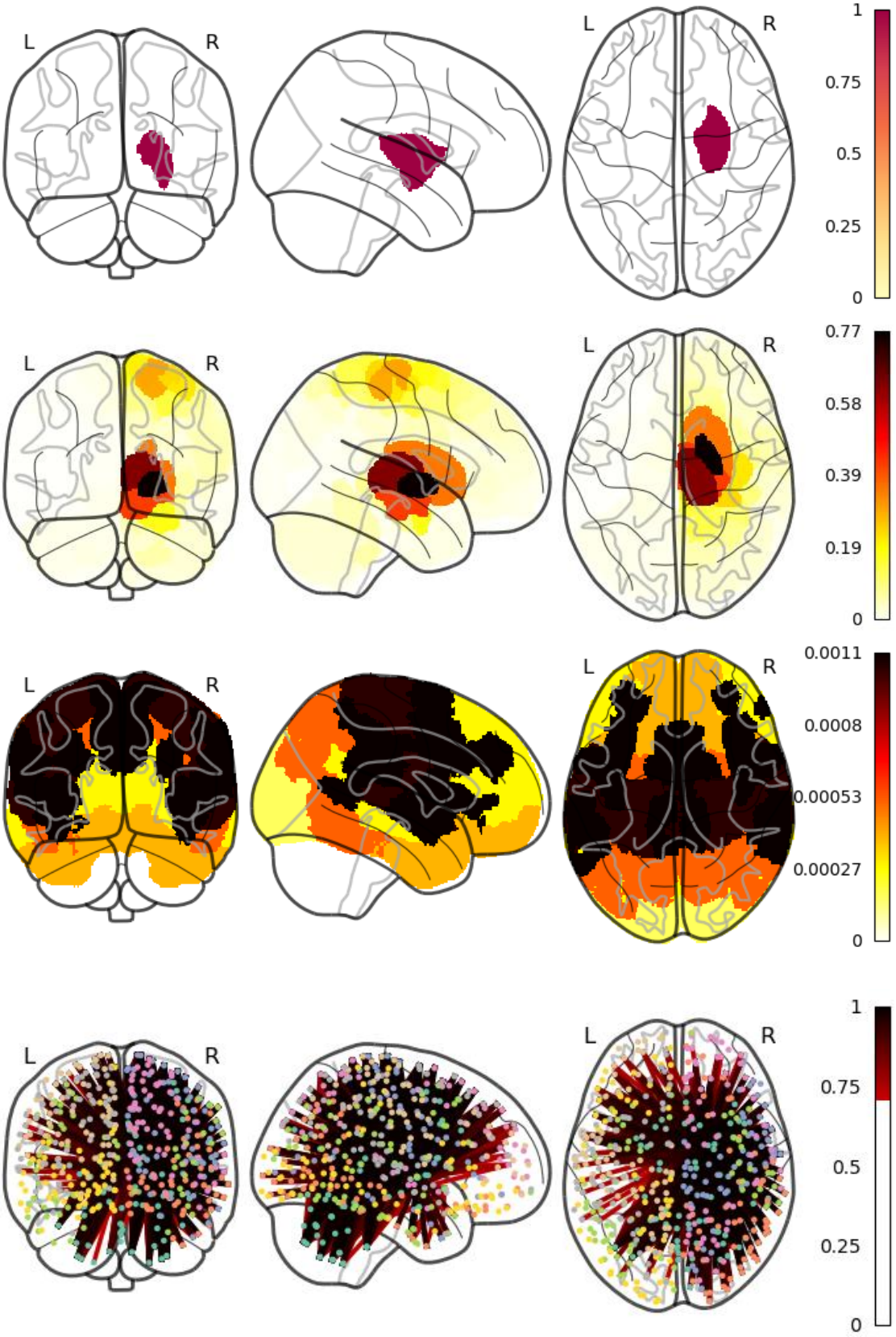

PATIENT 2 – Hischemic lesion right hemisphere

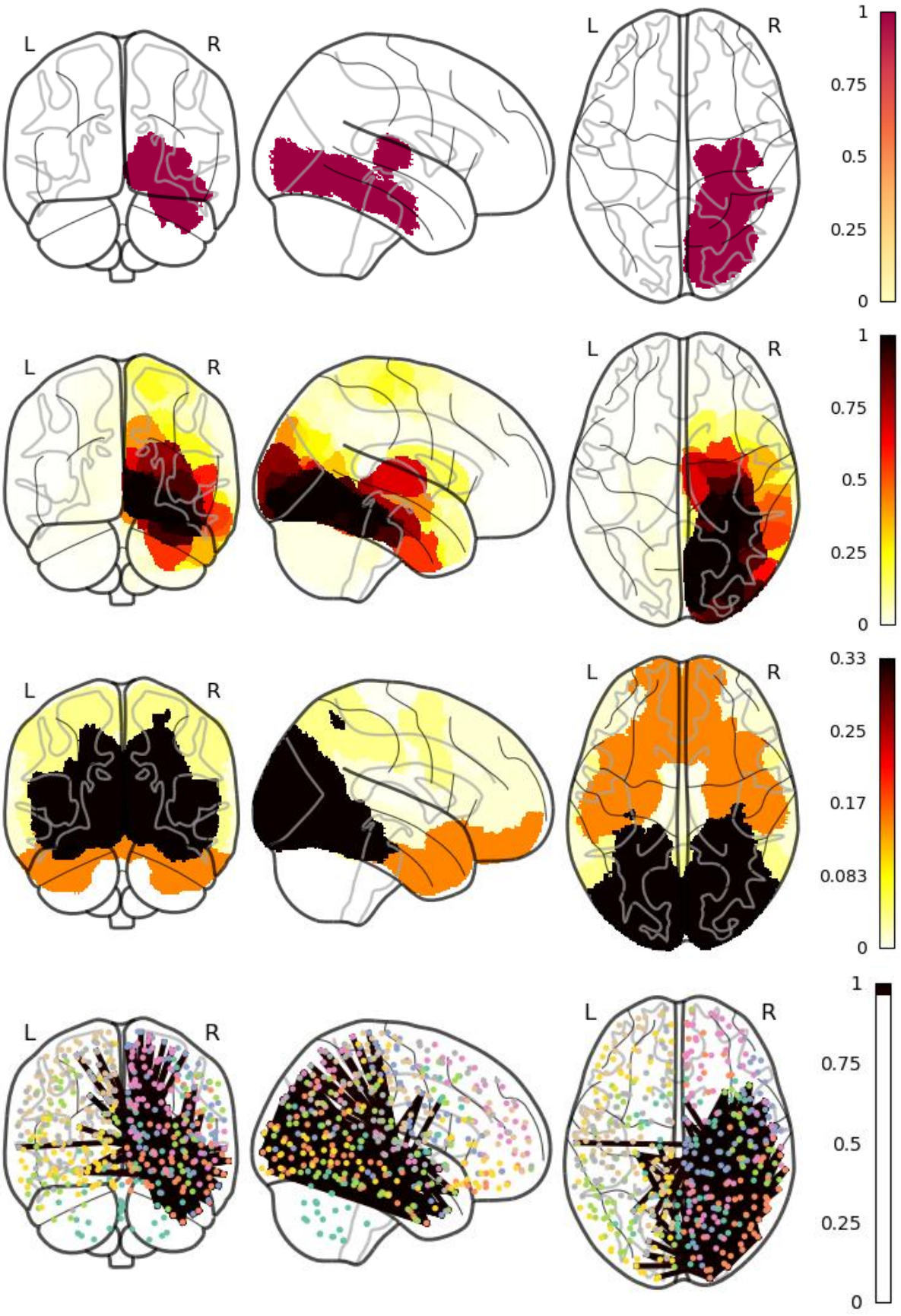

PATIENT 3 – Hischemic lesion right hemisphere

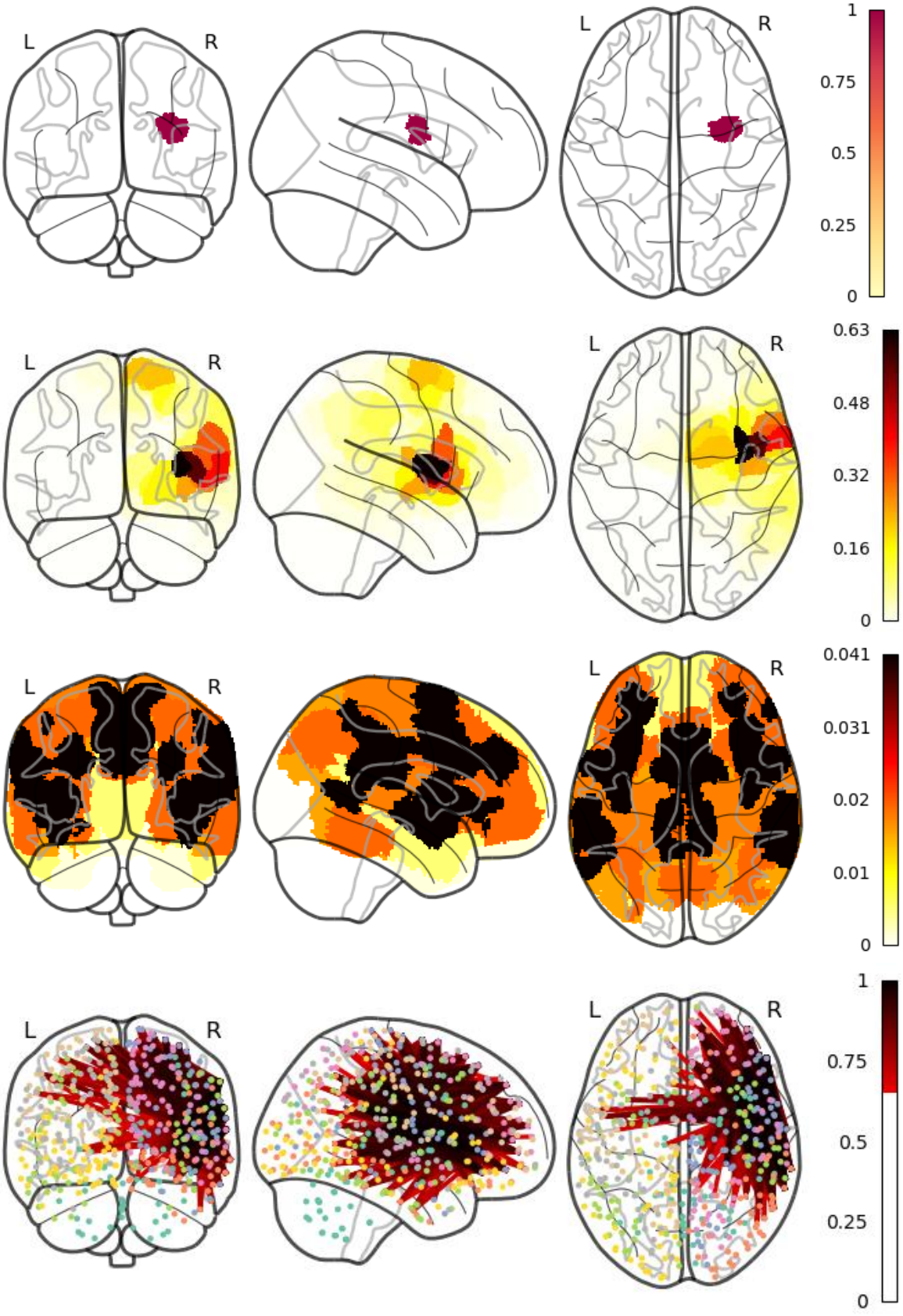

PATIENT 4 - Hischemic lesion left hemisphere